

A NEW CATALOG OF FARADAY ROTATION MEASURES AND REDSHIFTS FOR EXTRAGALACTIC RADIO SOURCES

ALISON M. HAMMOND, TIMOTHY ROBISHAW* & B. M. GAENSLER[†]

Sydney Institute for Astronomy, School of Physics, The University of Sydney, NSW 2006, Australia

* Covington Fellow, Dominion Radio Astrophysical Observatory, Herzberg Institute of Astrophysics, National Research Council Canada, PO Box 248,
 Penticton, BC, V2A 6J9, Canada

[†]bryan.gaensler@sydney.edu.au

Submitted to *The Astrophysical Journal Supplement Series*

ABSTRACT

We present a catalog of Faraday rotation measures (RMs) and redshifts for 4003 extragalactic radio sources detected at 1.4 GHz, derived by identifying optical counterparts and spectroscopic redshifts for linearly polarized radio sources from the NRAO VLA Sky Survey. This catalog is more than an order of magnitude larger than any previous sample of RM vs. redshift, and covers the redshift range $0 < z < 5.3$; the median redshift of the catalog is $z = 0.70$, and there are more than 1500 sources at redshifts $z > 1$. For 3650 of these sources at Galactic latitudes $|b| \geq 20^\circ$, we present a second catalog in which we have corrected for the foreground Faraday rotation of the Milky Way, resulting in an estimate of the residual rotation measure (RRM) that aims to isolate the contribution from extragalactic magnetic fields. We find no significant evolution of RRM with redshift, but observe a strong anti-correlation between RRM and fractional polarization, p , that we argue is the result of beam depolarization from small-scale fluctuations in the foreground magnetic field or electron density. We suggest that the observed variance in RRM and the anti-correlation of RRM with p both require a population of magnetized intervening objects that lie outside the Milky Way but in the foreground to the emitting sources.

Keywords: catalogs — galaxies: distances and redshifts, magnetic fields — magnetic fields — polarization

1. INTRODUCTION

Faraday rotation is a powerful probe of magnetic fields along the line of sight between a linearly polarized radio source and the observer. When combined with redshift information, Faraday rotation measurements provide the potential to constrain the evolution of cosmic magnetic fields over time scales corresponding to the redshifts of the most distant polarized sources detectable. However, previous studies of Faraday rotation measure (RM) vs. redshift have been hampered by the small size of the available samples (200–300 sources at most), often drawn from highly inhomogeneous data sets. Radio and optical surveys such as the NRAO Very Large Array Sky Survey (NVSS; Condon et al. 1998), and the Sloan Digital Sky Survey (SDSS; York et al. 2000) can enable a comprehensive new analysis of RM vs. redshift, thereby allowing much more sensitive studies of the evolution of magnetic fields over cosmic time.

1.1. Faraday Rotation

Faraday rotation is a birefringence effect whereby the linear polarization angle (θ) of a radio wave is rotated when propagating through a magnetized, ionized gas. For a distant linearly polarized radio source observed at a wavelength λ , the polarization angle is rotated by an amount $\Delta\theta = \text{RM} \lambda^2$, where RM is defined as:

$$\text{RM}(z_s) = 0.81 \int_{z_s}^0 \frac{n_e(z) B_{\parallel}(z) dl}{(1+z)^2} dz \text{ rad m}^{-2}. \quad (1)$$

In this Equation, z_s is the redshift of the polarized source; $n_e(z)$ is the free electron number density at some foreground redshift z , in cm^{-3} ; $B_{\parallel}(z)$ is the line-of-sight component of the magnetic field at redshift z , measured in μG ; and dl is a line-element along the line of sight, measured in parsecs. A positive RM corresponds to a magnetic field oriented toward the

observer. In the idealized case of a Faraday thin system, one can determine the RM by measuring values for θ at multiple observing wavelengths, and then performing a linear fit to θ vs. λ^2 .

Equation (1) implies that the observed RM is a superposition of contributions from multiple magneto-ionic regions along the entire line of sight. In every case, there is a contribution from the Earth's ionosphere ($\sim 1\text{--}2 \text{ rad m}^{-2}$; Brentjens & de Bruyn 2005), and for extragalactic sources there is always a foreground contribution from the Milky Way known as the Galactic Rotation Measure (GRM; $\sim 10\text{--}1000 \text{ rad m}^{-2}$, varying with Galactic longitude and latitude; Schnitzeler 2010; Oppermann et al. 2012). Outside of the Galaxy, there are many contributions to the observed RM, including the polarized sources themselves, intervening galaxies, their halos, intracluster gas or independent clouds of magnetized gas. The extragalactic component of RM can be studied by calculating the residual rotation measure (RRM), such that $\text{RRM} = \text{RM} - \text{GRM}$.

1.2. Previous Catalogs of RM and Redshift

Over the past several decades, there have been numerous studies in which RRM of polarized sources as a function of redshift have been used to probe extragalactic magnetic fields over cosmic time (Bernet et al. 2008; Fujimoto et al. 1971; Kronberg & Simard-Normandin 1976; Kronberg et al. 1977; Kronberg & Perry 1982; Kronberg et al. 2008; Nelson 1973; Oren & Wolfe 1995; Reinhardt 1972; Sofue et al. 1979; Thomson & Nelson 1982; Welter et al. 1984; You et al. 2003). These studies have demonstrated that the mean RRM of sources over the sky is zero out to redshifts $z > 4$. However, the variance of the RRM distribution, the effect of intervenors/absorbers and the precise nature of any RRM evolution with redshift all remain contentious. The largest sample reported to date is the (as-yet unpublished) data set ana-

lyzed by Kronberg et al. (2008), whose sample consisted of 268 RRM measurements for sources out to $z \sim 3.7$. These authors presented evidence for a significant increase in the variance of the RRM distribution as a function of increasing redshift, from which they proposed that galaxies hosted strong magnetic fields at relatively early times.

In the present paper, we use archival surveys and databases to derive a new catalog of RM and redshift for more than 4000 extragalactic radio sources out to redshifts $z \sim 5.3$, a sample that is markedly larger and extends to much higher redshifts than all previous efforts. We also present an additional catalog in which we have corrected for Galactic Faraday rotation for most sources, resulting in a compilation of RRM vs. z suitable for studies of the evolution of Faraday rotation and magnetic fields as a function of cosmic time. In §2 we describe the databases and surveys used in our analysis. In §3, we present our catalog of RM vs. z , while in §4 we present a catalog of RRM vs. z . In §5 we discuss the overall properties of the sample, and consider the relationships between RRM, fractional polarization and redshift for these sources.

2. DATABASES AND SURVEYS

In the following subsections, we describe the radio and optical data sets from which we obtained values of RM and z , respectively. The sky coverages of the surveys used in this study are indicated in Figure 1; the final catalog contains only sources with declinations $\delta \geq -40^\circ$, constrained by the coverage of the NVSS (from which all our RMs have been derived).

2.1. Obtaining Rotation Measures

The NVSS (Condon et al. 1998) was a 1.4 GHz radio survey that used the Very Large Array (VLA) to image the entire sky for $\delta \geq -40^\circ$ at an angular resolution $R \approx 45''$. The resulting source catalog contains information on Stokes parameters I , Q and U for over 1.8 million discrete objects.

The RMs that we use for our analysis come from the re-processing of the original NVSS data by Taylor et al. (2009), and are available online.¹ Taylor et al. (2009) used images of Stokes Q and U in two frequency bands at 1364.9 MHz and 1435.1 MHz for every NVSS source to determine linearly polarized intensity $P \equiv \sqrt{Q^2 + U^2}$ and fractional linear polarization $p \equiv P/I$. If the signal-to-noise ratio for P was greater than 8, they derived the RM from the difference in polarization position angle across the two bands. The resultant distribution of 37 543 RMs is provided in Figure 2. Because the RMs were derived only from two closely spaced frequency bands, the data are potentially subject to $n\pi$ ambiguities and non- λ^2 effects. However, subsequent broadband polarization studies for subsets of the Taylor et al. (2009) catalog have produced results that are in up to 96% agreement with the RMs derived by Taylor et al. (2009) (Mao et al. 2010; Van Eck et al. 2011; Law et al. 2011).

2.2. Obtaining Redshifts

Our sources of redshift data are two online databases plus several recent large optical redshift surveys. We exclude from consideration any objects flagged as stellar or Galactic. We also only use spectroscopic redshifts (as opposed to photometric redshifts or Lyman dropouts) due to the greater reliability and sufficient abundance of spectroscopic redshifts from the surveys we consider. Details on these databases and surveys are provided in §2.2.1 through §2.2.6.

¹ <http://www.ucalgary.ca/ras/rmcatalogue>

To assign redshifts to the RM catalog of Taylor et al. (2009), we need to make associations between sources detected at both optical and radio wavelengths. There have been numerous approaches to this issue (Magliocchetti et al. 1998; Ivezić et al. 2002; McMahon et al. 2002; Best et al. 2005; Sadler et al. 2007; Kimball & Ivezić 2008; Lin et al. 2010; Plotkin et al. 2010). Such studies use angular proximity as the primary discriminant in making an association between an optical source and a radio source, although the proximity requirement varies widely from $2''$ to $3'$, depending on the priority placed by different investigators on finding all genuine associations or minimizing false matches. Some authors have considered the possibility of multi-component sources with varying degrees of complexity, from merely incorporating double-lobed radio sources to consideration of all of double, triple, bent and core-jet scenarios (Magliocchetti et al. 1998; Best et al. 2005). Matching procedures also differ based on whether associations are made with a relatively low-resolution radio survey such as the NVSS ($R = 45''$), a high-resolution survey such as FIRST² ($R = 5''$; Becker et al. 1995; Ivezić et al. 2002), or a combination of both (Best et al. 2005; Plotkin et al. 2010). Some procedures make use of properties such as source size, flux or inclination between radio lobes (Magliocchetti et al. 1998; Best et al. 2005), while other methods calculate excess matches above those from random source distributions (Kimball & Ivezić 2008; Plotkin et al. 2010).

2.2.1. NED

The NASA/IPAC Extragalactic Database (NED; Helou et al. 1991, 1995)³ stores data on >170 million objects outside the Milky Way. NED includes 4 million sources with redshift information, including many associations between radio sources and optical redshifts. These data come from surveys, published results and references to known redshifts in the literature. We discarded any redshift that was not obtained spectroscopically, and also discard entries for which the “z Quality” field was flagged.

2.2.2. SIMBAD

The Set of Identifications, Measurements and Bibliography for Astronomical Data (SIMBAD; Wenger et al. 2000)⁴ is a database operated out of the Center de Données astronomiques de Strasbourg (CDS) in Strasbourg, France. It contains nearly five million Galactic and extragalactic objects. Like NED, SIMBAD includes redshift data for radio objects derived from surveys and from the literature.

2.2.3. SDSS

The SDSS⁵ (York et al. 2000) is an optical survey that has so far imaged more than one-third of the sky (14 500 square degrees) in five different wavebands at $R \approx 0.5''$, using a dedicated 2.5 m optical telescope at Apache Point, New Mexico. For the analysis in this paper we use data release 8 (DR8), released on 2011 January 11 (Aihara et al. 2011), which contains spectroscopic data (including redshifts) for

² The VLA Faint Images of the Radio Sky at Twenty centimeters survey (see §2.3 for more details).

³ <http://ned.ipac.caltech.edu/>, accessed on 2012 August 16.

⁴ <http://simbad.u-strasbg.fr/simbad/>, accessed on 2012 August 17.

⁵ <http://skyserver.sdss3.org/dr8/en/>

approximately 860 000 galaxies and 116 000 quasars over almost 9300 square degrees. We used Structured Query Language (SQL) to obtain data on spectroscopic redshifts and optical magnitudes for galaxies and quasars from the online DR8 database. We applied filters to our search to select only objects classified as galaxies or quasars, and to selectively remove any sources which had warnings associated with the redshift measurements.

2.2.4. The 6dFGS Survey

The Six-degree Field Galaxy Survey (6dFGS; Jones et al. 2004, 2009)⁶ measured the spectroscopic redshifts of 110 256 galaxies over 17 000 square degrees, with a median redshift $z = 0.053$. The survey used the 6dF fibre-fed multi-object spectrograph on the UK Schmidt telescope of the Australian Astronomical Observatory (AAO). We applied filters to our search to select only objects in the top two redshift quality bands, as determined by the survey (quality 3 or 4).

2.2.5. The 2dFGRS Survey

The Two-degree Field Galaxy Redshift Survey (2dFGRS; Colless et al. 2001, 2003)⁷ was carried out with the 2dF instrument on the Anglo-Australian Telescope (AAT). It covered approximately 1500 square degrees and obtained reliable redshifts for 221 414 galaxies at a median redshift $z = 0.11$. We applied filters to select only objects in the superior redshift quality bands, as determined by the survey (quality 3–5).

2.2.6. The 2QZ/6QZ Survey

The 2dF QSO Redshift survey (2QZ) and the 6dF QSO Redshift survey (6QZ)⁸ (Croom et al. 2004) were the quasar spectroscopic redshift survey counterparts, respectively, to the 2dFGRS and 6dFGS described above. In combination they are referred to as the 2QZ/6QZ survey. Combined, the 2QZ/6QZ survey contains redshift data for 23 660 quasars over 720 square degrees. We applied filters to select only objects with high-quality redshifts, as determined by the survey team (Quality_Flag_1 = 11, 21 or 31).

2.3. Morphological Information

We additionally make use of the higher angular resolution of the FIRST survey, with which we match radio sources with optical data using morphological information. The FIRST survey (Becker et al. 1995) consists of VLA images at 1.4 GHz covering 9900 deg², matched to the sky coverage of SDSS. FIRST detected approximately one million sources, and its high angular resolution ($R = 5''$ compared to $R = 45''$ for the NVSS) enables the detection of compact sources and provides detailed morphological information.

3. THE RM-REDSHIFT CATALOG

Previous catalogs of RM vs. z such as those presented by Welter et al. (1984), Oren & Wolfe (1995) and Kronberg et al. (2008) have suffered from a high degree of inhomogeneity. Typically, both RM and z data have been compiled from a range of small published (and occasionally unpublished) samples, which were then collated into an RM- z catalog. This approach was undertaken to maximize the size of the data set, although the results were still only catalogs

of 100–200 sources. With the wealth of new data available, we here attempt to strike a balance between creating a catalog with a large number of sources, while also maintaining a high degree of homogeneity in the data sets from which our information comes. To associate optical redshift data with the Taylor et al. (2009) RM catalog, we first identify sources for which associations had previously been made in NED or SIMBAD, and then use data from the optical redshift surveys described in §2.2 to make new associations.

3.1. NED and its Limitations

NED is currently the largest single database of extragalactic sources, and therefore represents the natural starting point to search for redshifts. A total of 2023 of the redshifts that we ultimately include in our RM-redshift catalog were provided from information in NED (50.5% of 4003 RM-redshift pairs). These represent cases for which a specific NVSS source has an associated redshift within the NED database.

Though many of the Taylor et al. (2009) NVSS sources are listed within NED, testing with the Sesame Name Resolver⁹ revealed that some NVSS sources are missing. Correspondence with the NED team (M. Schmitz, 2011, private communication) confirmed that only around 90% of the NVSS source catalog is in NED. The database is complete for right ascensions $0^h < RA < 5^h40^m$, but outside this range the coverage is incomplete. Inquiries revealed that source inclusion is being deferred until associations are made with preexisting entries in NED. This task has been ongoing for three years, with no firm completion date planned. Those sources not included have complications such as a single NVSS source being resolved into several FIRST sources or the presence of more than one object in the relevant field. Unfortunately, those sources not included are precisely those that are especially relevant for this project, as they are radio galaxies that have likely also been observed in the optical by spectroscopic surveys. We therefore make these associations ourselves, as described in §3.2.

3.2. A Radio-Optical Association Algorithm

We add to the redshifts for NVSS sources provided by NED and SIMBAD by associating the radio sources in the Taylor et al. (2009) catalog with redshifts from the four optical surveys described in §2.2. There are, however, a number of difficulties with making associations between optical and radio data. One significant example is galaxies which have complex radio morphologies, such as double-lobed structures, that are not mimicked in the optical. To help make these associations, we include data from the higher resolution FIRST survey (though some NVSS sources either lack a FIRST detection or lie outside the FIRST sky coverage). There is good complementarity between the high angular resolution of FIRST and the superior sensitivity of NVSS to extended emission (Best et al. 2005), allowing detection of both compact and multi-component radio sources.

Our association algorithm is primarily based on the work of Best et al. (2005), who tested and refined their criteria using Monte Carlo simulations involving catalogs of random sky locations. The association criteria arising from these simulations, based on the entire NVSS catalog of 1.8 million sources, were preferred to attempting to formulate new criteria using simulations on the much smaller subset of

⁶ <http://www-wfau.roe.ac.uk/6dFGS/>

⁷ <http://www2.aao.gov.au/2dFGRS/>

⁸ http://www.2dfquasar.org/Spec_Cat/catalogue.html

⁹ <http://cdsweb.u-strasbg.fr/cgi-bin/Sesame>

37 543 source listed by Taylor et al. (2009). We also incorporate aspects of the schemes of Magliocchetti et al. (1998), Ivezić et al. (2002), and McMahon et al. (2002); a summary of the main elements of our algorithm is represented in Figure 3. Excluding associations taken from NED and SIMBAD, the algorithm contributes 89% of the RM- z pairs in our RM-redshift catalog; the remainder were flagged by the algorithm as having complex features and were subsequently manually inspected.

3.2.1. Association Classes

Our algorithm associates sources and assigns them to one of five association classes, A, B, C, D or E, as summarized in Table 1. For sources in class A, we have used FIRST data to make the association; for sources in class B, we rely on NVSS data only (the particular limitations of class B are described in §3.5); class C corresponds to more complex sources that required manual visual inspection; class D corresponds to associations made within NED, while class E indicates associations made by SIMBAD. Class A is further subdivided into seven subclasses, A(i) through A(vii), depending on the radio morphology of the source in the FIRST data.

The admission criteria for association classes A to C are further explained below. Examples of sources in each of classes A(i), A(ii), A(iii), A(iv), A(v), A(vi), A(vii), B and C are provided in Figures 4, 5, 6, 7, 8, 9, 10, 11 and 12, respectively.

Following Best et al. (2005), we account for the possibility of multi-component NVSS sources by making an initial search of the Taylor et al. (2009) catalog in a $3'$ radius around each optical source. The distance of $3'$ is selected to ensure that genuine multi-component sources have at least two matches, while still being much less than the typical separation of $8' - 10'$ between NVSS sources. The chance of random matches within $3'$ is high, motivating more complex selection criteria as described below. As shown in Figure 3, our scheme automates associations in cases where there are fewer than three NVSS matches.

In cases for which there is one NVSS source within $3'$ of a given optical source, our algorithm checks for FIRST data within $30''$ of the optical position. If FIRST data are found and if the NVSS-optical offset is less than $15''$, the algorithm proceeds. A single NVSS source more than $15''$ from the optical source is not considered an association. The next steps taken by the algorithm depend on how many FIRST matches are found within $30''$.

A single FIRST match is accepted if the FIRST-optical offset is less than $3''$ [class A(i); see examples in Fig. 4] or if the FIRST-optical match is within $10''$ and is also within 75% of the major axis of the optical source [class A(ii); Fig. 5]. The rate of false detections for matches within $3''$ is estimated to be less than 1%, while the inclusion of matches within $10''$, subject to the additional criterion for class A(ii), helps maintain high completeness.

A double or triple match within FIRST is accepted if one of the two radio sources is within $3''$ of the optical galaxy [classes A(iii) and A(v), shown in Figs. 6 and 8, respectively] or if the doubles criterion is met for two of the matched FIRST sources [classes A(iv) and A(vi), shown in Figs. 7 and 9, respectively]. These require that the quantity $O \times S \times F$ is less than five, where O is the arcsecond offset between the optical galaxy and the mean position of two FIRST sources, S is the ratio of source size for those two FIRST sources, and F is their flux ratio. This derives from the finding of McMahon et al. (2002), that double-lobed radio sources detected in FIRST

have two lobes of similar sizes and fluxes, and a mean position that is close to the optical galaxy. The reliability of this procedure is estimated to be $> 99\%$.

Our scheme also treats the case where two NVSS sources are found within $3'$ of the same optical source. These sources are classified as potential double-lobed radio systems if a set of offset criteria are met: both radio sources must be within $90''$ of the optical galaxy, the mean position of the two radio sources must match the optical position within $15''$, and the nearer of the two radio components to the optical source must be $> 15''$ from the optical position (or there is less than $20''$ between the two radio components). We then search for FIRST data within $30''$. Best et al. (2005) did not consider sources in the absence of FIRST data, but noted the likely degree of contamination in the case of doubles if NVSS data alone are relied upon. For this work, the Taylor et al. (2009) catalog contains sufficiently few candidate doubles that those without clear FIRST data (i.e., a FIRST source within $3''$ of the optical source position) are visually inspected (see below). Potential doubles with clear FIRST data are associated as doubles and placed in class A(vii). Note that sources in class A(vii) have two NVSS sources (the two lobes of a radio galaxy) matched to the same optical source. Within the RM-redshift catalog, the two components of each pair are arbitrarily designated class A(vii)a or A(vii)b in reflection of this. Figure 10 shows two examples of class A(vii) associations.

In some cases for which there is only one NVSS match, there are no corresponding FIRST data because the source lies outside the sky coverage of the FIRST survey (see Figure 1), or because the source has faded between the NVSS and FIRST observations, or because a radio source seen as substantially extended in NVSS is resolved out in the higher angular resolution FIRST data. In these cases, a match is accepted if the NVSS-optical offset is less than $10''$, and the source is then placed in class B. Figure 11 shows two examples of class B sources. The choice of a $10''$ matching radius is conservative in light of other work, and avoids significant contamination from background sources (Best et al. 2005; Plotkin et al. 2010; Sadler et al. 2007). It is also smaller than the NVSS-optical offset limit of $15''$ that we use for class A (i.e., when a FIRST counterpart is detected).

For sources for which there are three or more NVSS matches, four or more FIRST matches, or a candidate double source with no clear FIRST data, the algorithm flags the optical source as requiring manual visual inspection. In these complex situations, images of the relevant parts of the sky are downloaded from the NVSS and FIRST postage stamp servers, the SDSS image server and the SuperCOSMOS image extraction service (for 2dFGRS, 6dFGS and 2QZ/6QZ). In cases for which we confirm visually that the optical and radio sources are associated, then the value for redshift from the optical survey is assigned to the Taylor et al. (2009) source, and these sources are assigned class C. Two examples of class C sources are shown in Figure 12. While visual inspection introduces some level of subjectivity to the resulting associations, we note that only 195 associations in our final RM-redshift catalog fall into this class, just 4.9% of the total.

3.2.2. Noteworthy Features of the Association Algorithm

In 25 cases (23 of which were drawn from 6dFGS), the algorithm matches two different sources from the same optical survey with a single radio source from Taylor et al. (2009). In all such cases, we visually inspected the optical and radio

images, using morphology and proximity to determine which optical source is associated with the radio source.

We note that while our association scheme attempts to use NVSS and FIRST together to achieve the best possible compromise between completeness and reliability, our approach does exhibit a slight bias against extended sources. This is because nearly all matches involving a single-component FIRST source are detected by our algorithm, while not all of those involving multiple NVSS components are identified (Best et al. 2005). There is no *a priori* reason that this slight bias should impact the results of our RM analysis.

3.3. Choosing a Final Redshift for the RM-Redshift Catalog

Many of the polarized sources in the Taylor et al. (2009) catalog have an optical counterpart and resulting redshift in more than one of the optical surveys or databases that we have considered. We list every such redshift in our RM-redshift catalog, but additionally identify a “selected redshift” for each Taylor et al. (2009) source, representing that redshift which we consider to be most reliable. For example, 59 NVSS sources have redshifts from two separate optical surveys, while one source was associated with three optical surveys. In 2296 cases, associations of Taylor et al. (2009) sources are made with both databases and surveys (for example, a Taylor et al. 2009 source that it is associated with an SDSS optical counterpart by our algorithm will sometimes have the same NVSS/SDSS match listed in NED), or an optical counterpart is listed both in NED and in SIMBAD. In many cases, the decision on a selected redshift is trivial, either because all redshift entries are the same (730 cases), or because all the associated redshifts agree closely with one another (1439 cases with $0 < \Delta z \leq 0.01$). From our total of 4003 sources, this leaves 127 cases for which multiple distinct redshifts are found, so that the selection of a final redshift could have a functional impact upon the catalog. The differing redshifts are due to disagreements between the constitutive surveys/databases. Some of these disagreements are attributable to identifiable errors such as measuring the redshift of an absorber along the line of sight to an emitter and wrongly assigning that redshift to the emitter.

In those cases where a substantive redshift selection needs to be made, the final selected redshift is chosen from among detections in multiple optical surveys/online catalogs in the descending priority listed in Table 2. This prioritization gives preference to surveys over databases, and prefers surveys with high angular resolution and wide-area sky coverage. NED is preferred to SIMBAD because of the greater number of reliable redshifts in NED.

3.4. Contents of the RM-Redshift Catalog

As described in §2.2 and §3, we have obtained redshifts for the polarized radio sources of Taylor et al. (2009) from a range of optical databases and surveys, with each optical/radio match given a corresponding association class as defined in Table 1. The resulting RM-redshift catalog contains 4003 sources with both RMs and redshifts (with a “selected” redshift listed in cases where multiple values for z have been found). This catalog contains an order-of-magnitude more entries than any previous compilation of RM vs. redshift, and extending out to much higher redshifts ($z = 5.27$). A sample of rows and columns from the RM-redshift catalog is shown in Table 3; the full RM-redshift catalog (available in its entirety as an online machine-readable table) contains the coordinates,

fractional polarization, RM and all other data for each source from Taylor et al. (2009), along with positions, redshifts, photometry, object types, journal references and association class derived for each optical match, and the selected redshift and other relevant data associated with the best-matching optical counterpart.

Table 4 shows the contents of the RM-redshift catalog broken down by survey and association class. The most common association class is A(i), representing a simple unresolved radio source that aligns closely with the corresponding optical counterpart. This is followed by class B, representing a similar situation to class A(i) but in cases either where no FIRST source is detected or no FIRST data are available. The 2dFGRS, 6dFGS and 2QZ/6QZ surveys provide most of their associations in class B, as their sky coverage has little overlap with FIRST. In contrast, almost all SDSS associations fall in class A, because the sky-coverages of FIRST and SDSS were intentionally matched. The total number of associations arising from each survey varies as expected according to the sky coverage and number of objects in each survey. For example, most survey associations are made with the SDSS, covering 9300 square degrees and containing almost 1 million extragalactic redshifts, while the fewest associations are made with 2QZ/6QZ, containing only 23 000 quasar redshifts and focusing on two small regions of the sky. The row labeled “Total” in Table 4 indicates the total number of matches to Taylor et al. (2009) for each survey or database, while the column labeled “All” indicates the total number of times each association class is assigned to a radio/optical match. The rows and columns labeled “Selected” show the contribution from each survey/database and from each association class, respectively, to the final selected redshifts using the priority order listed in Table 2.

3.5. Completeness, Reliability and Testing of Matching Processes

It is desirable to estimate both the completeness and the reliability (also known as efficiency; cf. Kimball & Ivezić 2008) of our RM-redshift catalog. Completeness refers to the fraction of real matches found, while reliability refers to the fraction of matches that are real. Both these quantities are difficult to estimate for our RM-redshift catalog because they are reliant upon a number of different factors: the completeness and proportion of spurious sources within each constituent survey, the number of true matches expected, and the level of background contamination in different regions of the sky.

Previous studies involving matches of NVSS with FIRST have found high completeness and reliability (Best et al. 2005; Kimball & Ivezić 2008). Kimball & Ivezić (2008) considered a range of matching radii; for the radius of $30''$ that we adopt, they found a completeness of 99.7% and a reliability of 96%. Matching between FIRST and SDSS yields a completeness above 94% and reliability above 90%. This rises further when NVSS data are included, with Best et al. (2005) suggesting 95% as a conservative completeness estimate.

Figure 13 shows the difference in NVSS and optical sky positions for matched radio-optical sources. The distributions of offsets in both Right Ascension and Declination are sharply peaked around zero, with a small spread. More than 90% of matched NVSS sources lie within $3''$ of the associated optical source; when double-lobed radio sources are excluded, this fraction rises to 94%.

One particular issue is the 375 sources in the RM-redshift catalog in association class B, i.e., sources that were asso-

ciated by our algorithm using optical and NVSS data only, without a FIRST detection. Class B associations are likely to be less reliable than those that also draw on FIRST data. Specifically, Best et al. (2005) have used Monte Carlo simulations to estimate that this association class may have a false detection rate of up to 6%. However, class B represents less than 10% of the entries in the RM-redshift catalog. Removing these sources would cause the completeness of the catalog to suffer, and also would further bias the sample against extended sources (due to the removal of extended sources that lie within the FIRST sky coverage but lack a FIRST detection). For the RM-redshift catalog as a whole, the simulations of Best et al. (2005) suggest that schemes that use both NVSS and FIRST have an overall reliability $> 98\%$.

We tested our algorithm using the prior radio-optical association work of Oren & Wolfe (1995) and Kimball & Ivezić (2008). Oren & Wolfe (1995) provided a small test sample of 20 sources that we used to test the basic functionality of our scheme. A more robust test involves the larger catalog of Kimball & Ivezić (2008), who associated the SDSS with a range of radio surveys, including the NVSS.¹⁰ Of the 37 354 Taylor et al. (2009) sources, 1295 appear with redshift data in the work of Kimball & Ivezić (2008).

The Kimball & Ivezić (2008) catalog used SDSS DR6 (Adelman-McCarthy et al. 2008), so we also performed tests using that data set, downloaded from the SDSS archive. Using the matching radii selected by Kimball & Ivezić (2008), which were different from our own due to the differing aims of that study, we were able to make 1260 of the 1295 associations made by Kimball & Ivezić (2008). The small differences are attributable to different correlation programs (the Kimball & Ivezić 2008 scheme, for instance, takes the FIRST data, not the optical data, for the position of the source), rounding differences arising from computation using different programs, and oddities within the Kimball & Ivezić (2008) catalog.

We also tested the robustness of our approach by randomly selecting 100 sources that had been associated via our algorithm, and visually inspecting them. In all cases, the visual inspection confirmed the association made by the code. This indicates that our algorithm associates optical and radio detections with a reliability $> 99\%$.

4. THE RRM-REDSHIFT CATALOG

4.1. Subtraction of the Galactic RM Contribution

In considering the evolution of magnetic fields over cosmic time, it is insufficient to simply plot RM against redshift because the foreground Faraday rotation from our own Milky Way must first be accounted for. This is especially important because the Galactic contribution is not uniform, but varies across the sky.

Due to the increased spatial fluctuations in the GRM at low Galactic latitudes, the first step in calculating RRM is to exclude all sources with $|b| < 20^\circ$ (drawing upon the study of these fluctuations by Schnitzeler 2010, and taking a threshold for $|b|$ comparable to that chosen for studies by Welter et al. 1984 and Oren & Wolfe 1995). We thus only calculate an RRM for 3650 of the 4003 sources presented in §3.4, the breakdown of which for each optical survey/database and for each association class is listed in the final row and final column of Table 4, respectively.

¹⁰ The Kimball & Ivezić (2008) catalog is available online at <http://www.astro.washington.edu/users/akimball/radiocat/>

A range of methods have been employed in the literature for calculating and subtracting the GRM. In this paper, we use the new map of the foreground Faraday sky computed by Oppermann et al. (2012), as shown in Figure 14. This map enables the calculation of an RRM by subtracting the GRM at that sky position from the RM value reported by Taylor et al. (2009). The Taylor et al. (2009) RM data were used in the construction of the Oppermann et al. (2012) map, but the reconstruction algorithm used in that work filters out the extragalactic contributions, ensuring that the resulting map is still appropriate to use in GRM calculations for Taylor et al. (2009) sources.

Figure 15 compares RM and RRM for our data. The efficacy of this GRM subtraction is indicated by the considerable narrowing of the RRM distribution (mean $+0.3 \pm 0.4 \text{ rad m}^{-2}$, standard deviation 23.2 rad m^{-2}) compared to the RM distribution (mean $+2.3 \pm 0.6 \text{ rad m}^{-2}$, standard deviation 36.1 rad m^{-2}). We also considered a number of previously published RRM schemes (Oren & Wolfe 1995; Johnston-Hollitt et al. 2004; Sofue et al. 1979; Short et al. 2007), but the GRM map of Oppermann et al. (2012) resulted by far in the smallest scatter in RRM of all approaches considered.

4.2. Contents of the RRM-Redshift Catalog

After applying the GRM correction discussed in §4.1, we derive a catalog of 3650 radio sources with both RRM and redshift. An extract of some columns from this RRM-redshift catalog can be seen in Table 5. The full RRM-redshift catalog (available online as a machine-readable table), contains the coordinates, flux, fractional polarization, RM, GRM, RRM, redshift, plus appropriate ancillary data for the radio source from Taylor et al. (2009) and for the best-matching optical counterpart.

This RRM-redshift catalog is more than an order of magnitude larger than any such catalog previously published. This is highlighted by Figure 16, in which we compare our catalog data against the samples of RRM vs. z described by Kronberg & Perry (1982), Welter et al. (1984) and Oren & Wolfe (1995).

5. ANALYSIS OF THE RRM-REDSHIFT CATALOG

5.1. Summary of Source Characteristics

The RRM-redshift catalog of 3650 sources covers a redshift range from 0 to 5.27, with a median redshift $z = 0.70$ and including almost 1400 sources with redshifts $z > 1$. The RRM-redshift catalog covers an RM range from -465.4 to $+270.4 \text{ rad m}^{-2}$, and an RRM range from -476.5 to $+206.1 \text{ rad m}^{-2}$. The RRM distribution, however, is tightly clustered around zero: 88% of sources have $|\text{RRM}| < 25 \text{ rad m}^{-2}$, 96% have $|\text{RRM}| < 50 \text{ rad m}^{-2}$, and 99.3% have $|\text{RRM}| < 100 \text{ rad m}^{-2}$. The 1.4 GHz Stokes I fluxes of the sample ranges from 11 mJy to 55 Jy, with a median of 300 mJy. Polarized fluxes range from 2.6 mJy to 1.3 Jy, with a median of 8 mJy.

The RRM-redshift catalog contains a diverse range of sources, drawn from several surveys and databases, and with a range of multi-wavelength properties and environments. A full analysis of this data set is beyond the scope of this paper, but here we present a brief analysis of its overall properties. To address potential issues of inhomogeneity in the catalog, we consider the full data set plus three relatively large and well-defined subsets: the 1376 sources for which the selected redshift was drawn from SDSS (referred to as

“SDSS sources” in subsequent discussion), the 516 sources with SDSS redshifts for which the optical spectrum was classified by SDSS as a galaxy (“SDSS galaxies”), and the 860 sources with SDSS redshifts for which the optical spectrum was classified by SDSS as a quasar (“SDSS quasars”).

For each of these four data sets, we consider three relationships: RRM as a function of z ; fractional linear polarization, p , as a function of z ; and RRM as a function of p . We note that any relation between RRM and p does not explicitly require knowledge of the redshift of the sources as has been the focus of this paper. However, because we have optical identifications, consideration can be given to how the RRM vs. p relation changes for different subsets of the overall data such as SDSS galaxies vs. SDSS quasars.

5.2. Residual Rotation Measure vs. Redshift

Figure 17 shows the distribution of RRM as a function of redshift for (a) the entire RRM-redshift catalog (this is the same data as shown in the bottom panels of Figs. 15 and 16), (b) all SDSS sources, (c) SDSS galaxies, and (d) SDSS quasars. As expected, there is a marked difference in the redshift distribution of SDSS galaxies (median redshift $z = 0.17$) compared to SDSS quasars (median redshift $z = 1.22$).

As indicated by the red lines overlaid on each panel of Figure 17, there is no apparent trend in the mean or standard deviation of RRM as a function of z in any of the four samples considered.¹¹ This is in strong contrast to the results of Kronberg et al. (2008), who presented a significant increase in the standard deviation of RRM to higher redshifts.

Kronberg et al. (2008) further characterized an evolution of RRM with z by splitting their data into two groups, corresponding to sources above and below a threshold redshift z_b . By applying a Kolmogorov-Smirnov (KS) test to the normalized cumulative distributions of $|\text{RRM}|$ at redshifts above and below z_b , Kronberg et al. (2008) found that the RRM of low- and high-redshift sources differed at 99% significance for $z_b \sim 1.8$. We can repeat this experiment with far larger sample sizes: in our RRM-redshift catalog, there are 3140 and 510 sources at $z_b < 1.8$ and $z_b \geq 1.8$, respectively. Applying a KS test to the distributions of $|\text{RRM}|$ on either side of this threshold, the values of $|\text{RRM}|$ for the two samples differ at 53% significance, which is consistent with the two groups of data being drawn from the same underlying distribution.

As a more sensitive test of any evolution of RRM with z , we use the Spearman rank test to look for evolution of $|\text{RRM}|$ as a function of z for all four data sets shown in Figure 17. We find no correlation for panel (c), and find a weak correlation between $|\text{RRM}|$ and z , at 2.5σ , 2.2σ and 3.8σ significance for panels (a), (b) and (d), respectively. We do not consider any of these trends significant, especially given that here and in further subsections below we are examining a diverse range of different possible correlations.

We thus conclude that there is no significant dependence of RRM or its variance as a function of z in our RRM-redshift catalog, in contrast to the strong effect of this kind reported previously using much smaller data sets (Welter et al. 1984; You et al. 2003; Kronberg et al. 2008). Recently, Bernet et al.

(2012) have considered a much smaller sample of 371 RMs from Taylor et al. (2009), and reported a similar inability to reproduce the RRM vs. z behaviour seen by Kronberg et al. (2008). Given this lack of redshift dependence, we now briefly consider possible origins of the observed RRM.

We first note two terms that must contribute to the standard deviation of 23.2 rad m^{-2} seen for the RRM in Figure 17(a): the measurement errors of the individual RMs in the Taylor et al. (2009) catalog, and the error associated with the GRM calculation of Oppermann et al. (2012). The standard deviation in RM due to measurement errors is 11 rad m^{-2} (Schnitzeler 2010; Stil et al. 2011), while the mean error in GRM for the sources in our RRM-redshift catalog is 6 rad m^{-2} . Subtracting these in quadrature from the observed variance leaves a standard deviation of 20 rad m^{-2} that must come from one or more astrophysical phenomena.

An obvious explanation for the lack of redshift evolution is that the RRM is solely a residual contribution from the Milky Way, resulting from imperfect foreground subtraction, or from RM fluctuations on smaller angular scales than are being sampled by the GRM map of Oppermann et al. (2012). We can rule out the former option, because while the RMs of our sources show a strong dependence on Galactic longitude and latitude (as seen in Fig. 2 for the larger NVSS RM sample from which our catalog is derived), the corresponding RRM show no pattern or trend with Galactic coordinates. To consider the latter option, we note that the typical spacing between the sources that Oppermann et al. (2012) used to calculate their foreground map is $\sim 1^\circ$, meaning that any Galactic contribution to our observed RRM must represent GRM fluctuations on angular scales $\lesssim 1^\circ$. Stil et al. (2011) calculate the fluctuations in GRM on these scales and show that, at latitudes $|b| \geq 20^\circ$ as we are considering here, the standard deviation in RM on a scale of 1° is $12\text{--}17 \text{ rad m}^{-2}$. Subtracting this Galactic term in quadrature from our observed variance implies that there is a $10\text{--}15 \text{ rad m}^{-2}$ contribution to the standard deviation in RRM that cannot be due to small-scale fluctuations in GRM, and hence must be extragalactic. This can be compared with the work of Schnitzeler (2010), who performed a statistical decomposition of the RMs in the Taylor et al. (2009) catalog into different components as a function of Galactic latitude, and concluded that extragalactic Faraday rotation contributed a standard deviation of $\approx 6 \text{ rad m}^{-2}$ to the RMs of Taylor et al. (2009). An agreement within a factor of ~ 2 between our estimate and that of Schnitzeler (2010) seems reasonable given the very different approaches taken between the two studies.

We now consider the possibility that most of the extragalactic contribution to RRM arises in the polarized sources themselves, e.g., in an envelope of ionized gas in the host galaxy or in its immediate environment. If the RRM originates at the same redshift as the emitter, then we expect a $(1+z)^{-2}$ dilution factor as per Equation (1). The corresponding contribution to the variance in RRM should then decrease with redshift in Figure 17 (cf. the dashed line in Fig. 7 of Kronberg et al. 2008). Specifically, if we assume that the extragalactic contribution to the standard deviation in RRM of $10\text{--}15 \text{ rad m}^{-2}$ corresponds to sources at our median redshift $z = 0.7$, then an identical population of sources at a redshift $z = 2$ should only contribute a standard deviation in RRM of $1\text{--}2 \text{ rad m}^{-2}$. Considered in quadrature with the other terms contributing to the scatter in RRM as discussed above, this dilution should result in an overall decrease in the standard deviation of RRM by

¹¹ The two places in Figure 17(a) where the standard deviation is substantially larger than $\approx 20\text{--}25 \text{ rad m}^{-2}$ are produced entirely from two sources with anomalously large RRM (a source at $z = 1.44$ with $\text{RRM} = -444 \text{ rad m}^{-2}$ and a source at $z = 2.13$ with $\text{RRM} = -476 \text{ rad m}^{-2}$, respectively). The latter source is an SDSS quasar, and so also has an effect on the standard deviations in panels (b) and (d).

2–4 rad m⁻² between $z = 0.7$ and $z = 0.2$. Although this is a small effect, we can rule out its presence in our data — the Spearman rank test discussed above shows that if anything, the variance in RRM slightly increases, not decreases, with redshift. The lack of evolution of RRM with z can then only be explained if the standard deviation in RRM evolves with $(1+z)^2$ in the emitter’s reference frame, to cancel out the $(1+z)^{-2}$ effect as the signal propagates to Earth. This would be a fortuitous coincidence and would also represent very strong evolution of the emitted RRM with redshift, both of which make this possibility unlikely.

The alternative is that the extragalactic component of RRM towards each source is introduced in one or more intervening systems along the line of sight between the polarized source and the observer, a possibility considered in detail by many previous authors (e.g., Bernet et al. 2008; Kronberg et al. 2008; Oren & Wolfe 1995; Welter et al. 1984). If the intervening systems are all at comparable redshifts, then we will not see a $(1+z)^{-2}$ dilution term, and indeed might expect a slight increase in variance of RRM with increasing z , since more distant sources are more likely to have an intervenor along the line of sight (see solid and dotted lines in Fig. 7 of Kronberg et al. 2008). Kronberg et al. (2008) advocate a population of intervenors with a standard deviation of RRM of ~ 60 – 115 rad m⁻² in the observer’s frame, but our analysis argues that a contribution 10–15 rad m⁻² is more likely. This is broadly consistent with the halo of a Milky-Way-like galaxy ($n_e \approx 3 \times 10^{-4}$ cm⁻³, $B \approx 1$ μ G, $l \approx 50$ kpc; Gaensler et al. 2008; Mao et al. 2010; Sun & Reich 2012), but a proper interpretation requires further, detailed consideration of this and other possible intervening source populations.

5.3. Polarized Fraction vs. Redshift

Figure 18 shows how p varies with z for the entire RRM-redshift catalog, for all SDSS sources, for SDSS galaxies, and for SDSS quasars. Panels (a) and (b) show a clear trend, in that sources with $z \lesssim 0.5$ can have a range of polarized fractions extending beyond $p = 30\%$, while sources at $z \gtrsim 0.5$ are confined solely to lower polarized fractions, $p \sim 5\%$.

Panels (c) and (d) provide a simple explanation for this apparent bimodality. Within the SDSS sub-sample, the low-redshift sources that can be both weakly or strongly polarized are all classified as galaxies based on their optical spectra. In contrast, the SDSS sources that extend to high redshifts and that are all relatively weakly polarized all have optical spectra indicating that they are quasars. While this distinction needs further study, a likely explanation is that the NVSS counterparts to the SDSS galaxies are radio lobes from active galaxies, which are expected to be Faraday thin and thus show high degrees of polarization. In contrast, the NVSS counterparts to SDSS quasars are radio-loud cores, for which optical depth effects and strong magnetic fields are expected to result in reduced polarization levels.

We can confirm this hypothesis by considering the distribution of association classes for the SDSS galaxies compared to the SDSS quasars. As summarized in Table 1, the most robust classifications are class A, in which an NVSS source has a clear match with an optical counterpart and also shows a relatively simple morphology in FIRST. Within class A, subclasses A(i) and A(ii) are characteristic of core-dominated radio morphologies, while classes A(iii) through A(vii) represent radio morphologies for which a significant fraction of the emission is from radio lobes. If the radio polarization from

SDSS galaxies is mainly from radio lobes and that from SDSS quasars is mainly from radio cores, then we expect the SDSS galaxies to be dominated by classes A(iii) to A(vii), while the SDSS quasars should be dominated by classes A(i) and A(ii). Indeed the data support this expectation: considering only SDSS sources in class A, 35% of SDSS galaxies are in classes A(i) and A(ii), while 65% are in classes A(iii) through A(vii). In contrast, 54% of SDSS quasars are in classes A(i) and A(ii), while 46% are in classes A(iii) to A(vii). Furthermore, we note that class C corresponds to complex, extended morphologies that cannot be classified automatically. For SDSS galaxies, 20% of all sources in the RRM-redshift catalog are in class C, while for SDSS quasars, the fraction of class C sources drops to just 8%. All this additional morphological information clearly demonstrates that SDSS galaxies are dominated by lobes, while SDSS quasars are dominated by cores, consistent with the differing distributions of fractional polarization for these two populations seen in Figure 18.

Noting the differing polarization properties of galaxies and quasars, we can then consider whether there is any evolution of p with z in Figures 18(c) and (d). Applying the Spearman rank test, we find no significant correlation of p with z for either SDSS galaxies or SDSS quasars, as apparent by eye via the red lines marking the mean and standard deviation of p as a function of z . A similar absence of evolution of p with z at 1.4 GHz was recently found by Banfield et al. (2011) from a smaller sample of 69 sources in the redshift range $0.04 < z < 3.2$.

Other studies of polarization as a function of redshift have usually considered parameters such as the “depolarization measure” (DP; the ratio of p at a high frequency to that at a low frequency) or $\lambda_{1/2}$ (the wavelength at which p falls to half its peak value) (e.g., Kronberg et al. 1972; Goodlet et al. 2004). Many of these studies have found that DP increases with z or that $\lambda_{1/2}$ decreases with z , in both cases indicating increased depolarization at higher redshifts (Conway et al. 1974; Goodlet et al. 2004; Goodlet & Kaiser 2005; Inoue & Tabara 1982; Kronberg et al. 1972). While we do not see such an effect here, it is important to note that such studies convert observed values of DP or $\lambda_{1/2}$ to those seen in the reference frame of the emitter. We cannot make such a correction for our sample because we do not have multi-wavelength information that would tell us how p depends on wavelength for each source. With the exception of the study of Banfield et al. (2011), our result is thus not directly comparable with previous work on the depolarization of radio sources as a function of redshift, without the inclusion of several additional assumptions.

5.4. Residual Rotation Measure vs. Polarized Fraction

In Figure 19 we plot the dependence of RRM on p for the entire RRM-redshift catalog, for all SDSS sources, for SDSS galaxies, and for SDSS quasars. In this case we see a striking pattern in all four panels: the standard deviation in RRM is large for low fractional polarizations, and is small for high fractional polarizations.

We first note that this is not an artifact of sensitivity and signal-to-noise. The uncertainty in an individual RM measurement (and hence the variance in a large sample of similar RM measurements) is inversely proportional to the signal-to-noise ratio (Brentjens & de Bruyn 2005). Thus we expect a source with a low polarized flux to have a large error in RM, and vice versa. However, we are here plotting the fractional

polarization rather than the polarized flux, and there is no correlation between these two parameters in our catalog. (If anything, any bias is in the reverse direction, since the faintest sources can only be detected in polarization if their fractional polarization is high.) The behavior seen in Figure 19 is thus astrophysical, rather than instrumental.

The most likely interpretation for this behavior is a depolarization mechanism, since stronger Faraday effects in or in front of a polarized source can induce reduced polarization through a variety of mechanisms (e.g., Burn 1966; Gardner & Whiteoak 1966; Tribble 1991; Sokoloff et al. 1998). Bandwidth depolarization cannot be a contributor in Figure 19, since this effect is only significant for RMs with magnitudes larger than $\sim 100 \text{ rad m}^{-2}$ (see Fig. 1 of Taylor et al. 2009). Just 2% of the sources in our RRM-redshift catalog have $|\text{RM}| > 100 \text{ rad m}^{-2}$, so this cannot be a significant contributor to the observed depolarization. Depth depolarization is also unlikely to be a factor, since this only occurs when the emitting medium is mixed with the medium producing the Faraday rotation. We discussed in §5.2 above how the lack of evolution of RRM with z argues against an intrinsic origin for the RRM, meaning that the RRM signal occurs wholly in the foreground to the polarized sources and so cannot produce depth depolarization.

The remaining possibility is beam depolarization, whereby high values of RRM imply large fluctuations in RRM on scales smaller than the angular extent of the radio source (even in cases where the source is unresolved by the telescope beam). Such fluctuations will cause differing polarization angles within the beam to cancel, resulting in a reduced polarized fraction.

Haverkorn et al. (2008) have shown that the Galactic foreground can indeed simultaneously produce larger RMs and enhanced beam depolarization against unresolved polarized background sources. Beam depolarization due to the Galactic foreground produces an anti-correlation between GRM and p (Haverkorn et al. 2008), and so thus can possibly produce a dependence between RRM and p given that one component of RRM is likely to be a residual Galactic contribution produced by small-scale fluctuations in GRM (see §5.2). While the depolarizing effects of the Galaxy are likely to be present in our data, they are insufficient on their own to explain the trend that we see between $|\text{RRM}|$ and polarized fraction. For example, Figure 6 of Haverkorn et al. (2008) shows that for similar angular resolution and observing frequency to those of the NVSS data being considered here, fluctuations in Galactic RM at the level of $\sim 200 \text{ rad m}^{-2}$ are needed to depolarize background sources by a factor of ~ 2 . In contrast, Figure 19 suggests that fluctuations in RRM only of magnitude $\sim 50 \text{ rad m}^{-2}$ can depolarize background sources by a factor of ~ 3 – 5 . The depolarization that we observe is thus too strong an effect to be explained only by small-scale Galactic RM fluctuations. The beam depolarization also does not seem to be originating in the emitting sources themselves, since we have argued in §5.2 above that the RRM does not have a significant intrinsic component. A significant contribution to the observed depolarization must therefore be due to small-scale fluctuations in RM somewhere between the source and the Milky Way, in intervening magneto-ionic material along the line of sight. This is the same origin independently proposed in §5.2 for the extragalactic component of the RRM themselves. Bernet et al. (2012) have used a different approach, focusing on the frequency dependence of depolarization, but

have separately come to a similar conclusion that the extragalactic intervenors contributing to the observed RRM must be highly turbulent.

6. CONCLUSIONS

We have compared the extragalactic rotation measure catalog of Taylor et al. (2009) with redshift data from a range of optical surveys and databases to produce a new sample of 4003 sources with both RM and redshift data (the “RM-redshift catalog”). We further derive a catalog of residual rotation measure vs. redshift, in which we have subtracted the Galactic RM contribution toward a subset of 3650 high-latitude sources (the “RRM-redshift catalog”). The resulting samples contain more than an order of magnitude more sources than any previously published catalogs of RM vs. redshift or RRM vs. redshift.

In our RRM-redshift catalog, we do not see any significant evidence that the variance of RRM changes with redshift, in contrast to previous studies by Welter et al. (1984) and Kronberg et al. (2008) who found that the RRM of their sources showed increased scatter at higher z . The overall standard deviation of the RRM in our catalog is 23 rad m^{-2} , of which 13 rad m^{-2} is due to errors associated with measurement and foreground removal, 12 – 17 rad m^{-2} is due to residual small-scale fluctuations in the Galactic RM, and 10 – 15 rad m^{-2} is extragalactic Faraday rotation that is not intrinsic to the emitting source and must originate in intervening systems between the radio sources and the Milky Way.

We find a strong distinction between the fractional polarizations of radio sources whose optical counterparts are galaxies and those whose optical counterparts are quasars. The former can be highly polarized, representing the extended lobes of radio galaxies, while the latter are only weakly polarized, representing the radio cores of active galaxies. Beyond this bimodality, we find no evolution of polarized fraction with redshift for either the galaxy or quasar population considered separately.

Finally, we identify a strong depolarization effect in our RRM-redshift catalog, whereby sources with even modest residual Faraday rotation, $|\text{RRM}| \gtrsim 20 \text{ rad m}^{-2}$, have substantially reduced polarized fractions compared to sources with RRM near 0 rad m^{-2} . We interpret this as beam depolarization due to small-scale fluctuations in magnetic field strength and gas density in the same intervening population that contributes to the RRM.

A full consideration of the nature of the extragalactic source population that produces the observed Faraday rotation and depolarization is beyond the scope of this paper, but future investigations should consider the relationship of RRM with z for different sub-populations, and should study the dependence of the observed depolarization on wavelength, observing frequency and angular resolution. Our analysis highlights the limitations imposed by the contribution of the Galactic foreground RM, even in cases where the foreground is modeled with a sophisticated algorithm that uses more than 40 000 RMs as input. A much denser RM grid, with each RM determined far more robustly than from the two frequency channels of NVSS data used here, is required to accurately account for the foreground contribution and to identify subtle trends of polarization properties with redshift. Such a data set will be provided by the upcoming Polarization Sky Survey of the Universe’s Magnetism (POSSUM) on the Australian Square Kilometre Array Pathfinder (Gaensler et al. 2010). This next

generation of polarization data will be a powerful discriminant between different mechanisms for extragalactic Faraday rotation measure and depolarization, and can thus provide sensitive probes of magnetic field and electron density as a function of cosmic time.

We are indebted to Marion Schmitz for extraordinary levels of assistance in using the NED database. We also thank Larry Rudnick, Paul Hancock, Helen Johnston, John Ching, Elaine Sadler, Scott Croom and Julia Bryant for useful discussions, and acknowledge valuable email correspondence with Ani Thakar, Benjamin Alan Weaver, Harold Corwin, Landais Gilles, Marc Wenger, Francois Ochsenbein, Amy Kimball, Jim Condon and Matthew Colless. B. M. G. and T. R. acknowledge the support of the Australian Research Council through grants FF0561298, FL100100114 and FS100100033. This research has made use of: the SIMBAD database, operated at Centre de Données astronomiques de Strasbourg, France; the NASA/IPAC Extragalactic Database (NED) which is operated by the Jet Propulsion Laboratory, California Institute of Technology, under contract with NASA; NASA's Astrophysics Data System Abstract Service; the SDSS, for which funding has been provided by the Alfred P. Sloan Foundation, the Participating Institutions, the National Science Foundation, and the U.S. Department of Energy Office of Science; the 2dF/6dF QSO Redshift Surveys (2QZ/6QZ), which were compiled by the 2QZ/6QZ teams from observations made with the 2-degree Field and 6-degree Field on the Anglo-Australian Telescope; and the IDL Astronomy User's Library at Goddard Space Flight Center (available at <http://idlastro.gsfc.nasa.gov/>). Some of the results in this paper have been derived using the HEALPix (Górski et al. 2005) package. The National Radio Astronomy Observatory is a facility of the National Science Foundation operated under cooperative agreement by Associated Universities, Inc.

Facilities: AAT Sloan UKST VLA

REFERENCES

- Adelman-McCarthy, J. K. et al. 2008, *ApJS*, 175, 297
 Aihara, H. et al. 2011, *ApJS*, 193, 29
 Banfield, J. K., George, S. J., Taylor, A. R., Stil, J. M., Kothes, R., & Scott, D. 2011, *ApJ*, 733, 69
 Becker, R. H., White, R. L., & Helfand, D. J. 1995, *ApJ*, 450, 559
 Bernet, M. L., Miniati, F., & Lilly, S. J. 2012, *ApJ*, in press (arXiv:1209.2410)
 Bernet, M. L., Miniati, F., Lilly, S. J., Kronberg, P. P., & Dessauges-Zavadsky, M. 2008, *Nature*, 454, 302
 Best, P. N., Kauffmann, G., Heckman, T. M., & Ivezić, Ž. 2005, *MNRAS*, 362, 9
 Brentjens, M. A. & de Bruyn, A. G. 2005, *A&A*, 441, 1217
 Burn, B. J. 1966, *MNRAS*, 133, 67
 Colless, M. et al. 2001, *MNRAS*, 328, 1039
 —. 2003, arXiv:astro-ph/0306581
 Condon, J. J., Cotton, W. D., Greisen, E. W., Yin, Q. F., Perley, R. A., Taylor, G. B., & Broderick, J. J. 1998, *AJ*, 115, 1693
 Conway, R. G., Haves, P., Kronberg, P. P., Stannard, D., Vallee, J. P., & Wardle, J. F. C. 1974, *MNRAS*, 168, 137
 Croom, S. M., Smith, R. J., Boyle, B. J., Shanks, T., Miller, L., Outram, P. J., & Loaring, N. S. 2004, *MNRAS*, 349, 1397
 Fujimoto, M., Kawabata, K., & Sofue, Y. 1971, *Progr. Theor. Phys. Suppl.*, 49, 181
 Gaensler, B. M., Landecker, T. L., & Taylor, A. R. 2010, *BAAS*, 42, 470.13
 Gaensler, B. M., Madsen, G. J., Chatterjee, S., & Mao, S. A. 2008, *PASA*, 25, 184
 Gardner, F. F. & Whiteoak, J. B. 1966, *ARA&A*, 4, 245
 Goodlet, J. A. & Kaiser, C. R. 2005, *MNRAS*, 359, 1456
 Goodlet, J. A., Kaiser, C. R., Best, P. N., & Dennett-Thorpe, J. 2004, *MNRAS*, 347, 508
 Górski, K. M., Hivon, E., Banday, A. J., Wandelt, B. D., Hansen, F. K., Reinecke, M., & Bartelmann, M. 2005, *ApJ*, 622, 759
 Haverkorn, M., Brown, J. C., Gaensler, B. M., & McClure-Griffiths, N. M. 2008, *ApJ*, 680, 362
 Helou, G., Madore, B. F., Schmitz, M., Bica, M. D., Wu, X., & Bennett, J. 1991, *Astrophys. Space Sci. Library*, 171, 89
 Helou, G., Madore, B. F., Schmitz, M., Wu, X., Corwin Jr, H. G., Lague, C., Bennett, J., & Sun, H. 1995, *Astrophys. Space Sci. Library*, 203, 95
 Inoue, M. & Tabara, H. 1982, in *IAU Symposium*, Vol. 97, *Extragalactic Radio Sources*, ed. D. S. Heeschen & C. M. Wade, 339
 Ivezić, Ž. et al. 2002, *AJ*, 124, 2364
 Johnston-Hollitt, M., Hollitt, C. P., & Ekers, R. D. 2004, in *The Magnetized Interstellar Medium*, ed. B. Uyaniker, W. Reich, & R. Wielebinski, 13–18
 Jones, D. H. et al. 2009, *MNRAS*, 399, 683
 —. 2004, *MNRAS*, 355, 747
 Kimball, A. E. & Ivezić, Ž. 2008, *AJ*, 136, 684
 Kronberg, P. P., Bernet, M. L., Miniati, F., Lilly, S. J., Short, M. B., & Higdon, D. M. 2008, *ApJ*, 676, 70
 Kronberg, P. P., Conway, R. G., & Gilbert, J. A. 1972, *MNRAS*, 156, 275
 Kronberg, P. P. & Perry, J. J. 1982, *ApJ*, 263, 518
 Kronberg, P. P., Reinhardt, M., & Simard-Normandin, M. 1977, *A&A*, 61, 771
 Kronberg, P. P. & Simard-Normandin, M. 1976, *Nature*, 263, 653
 Law, C. J. et al. 2011, *ApJ*, 728, 57
 Lin, Y.-T., Shen, Y., Strauss, M. A., Richards, G. T., & Lunnan, R. 2010, *ApJ*, 723, 1119
 Magliocchetti, M., Maddox, S. J., Lahav, O., & Wall, J. V. 1998, *MNRAS*, 300, 257
 Mao, S. A., Gaensler, B. M., Haverkorn, M., Zweibel, E. G., Madsen, G. J., McClure-Griffiths, N. M., Shukurov, A., & Kronberg, P. P. 2010, *ApJ*, 714, 1170
 McMahon, R. G., White, R. L., Helfand, D. J., & Becker, R. H. 2002, *ApJS*, 143, 1
 Nelson, A. H. 1973, *PASJ*, 25, 489
 Oppermann, N. et al. 2012, *A&A*, 542
 Oren, A. L. & Wolfe, A. M. 1995, *ApJ*, 445, 624
 Plotkin, R. M. et al. 2010, *AJ*, 139, 390
 Reinhardt, M. 1972, *A&A*, 19, 104
 Sadler, E. M. et al. 2007, *MNRAS*, 381, 211
 Schnitzeler, D. H. F. M. 2010, *MNRAS*, 409, L99
 Short, M. B., Higdon, D. M., & Kronberg, P. P. 2007, *Bayesian Analysis*, 2, 665
 Sofue, Y., Fujimoto, M., & Kawabata, K. 1979, *PASJ*, 31, 125
 Sokoloff, D. D., Bykov, A. A., Shukurov, A., Berkhuijsen, E. M., Beck, R., & Poezd, A. D. 1998, *MNRAS*, 299, 189
 Stil, J. M., Taylor, A. R., & Sunstrum, C. 2011, *ApJ*, 726, 4
 Sun, X. H. & Reich, W. 2012, *A&A*, 543, A127
 Taylor, A. R., Stil, J. M., & Sunstrum, C. 2009, *ApJ*, 702, 1230
 Thomson, R. C. & Nelson, A. H. 1982, *MNRAS*, 201, 365
 Tribble, P. C. 1991, *MNRAS*, 250, 726
 Van Eck, C. L. et al. 2011, *ApJ*, 728, 97
 Welter, G. L., Perry, J. J., & Kronberg, P. P. 1984, *ApJ*, 279, 19
 Wenger, M. et al. 2000, *A&AS*, 143, 9
 York, D. G. et al. 2000, *AJ*, 120, 1579
 You, X. P., Han, J. L., & Chen, Y. 2003, *Acta Astron. Sinica*, 44, 155

Table 1
Association classes between NVSS radio sources of Taylor et al. (2009) and their optical counterparts.

Class	Description
A	Match using FIRST
A(i)	Close core match with FIRST
A(ii)	Core match with FIRST
A(iii)	Single NVSS; closely matched double in FIRST
A(iv)	Single NVSS; double in FIRST
A(v)	Single NVSS; closely matched triple in FIRST
A(vi)	Single NVSS; triple in FIRST
A(vii)	Double-lobed in NVSS with FIRST
B	Core match in NVSS; either no FIRST detection or no FIRST data
C	Manual visual identification
D	Association made in NED
E	Association made in SIMBAD

Table 2
Prioritization of surveys and databases in selecting a final redshift, in cases where a radio source from Taylor et al. (2009) has matches in more than one optical redshift catalog.

Priority	Survey or Database
1	SDSS
2	6dFGS
3	2dFGRS
4	2QZ/6QZ
5	NED
6	SIMBAD

Table 3
Selected Columns from Our RM-Redshift Catalog of Polarized Radio Sources with Optical Counterparts

NVSS ID	SDSS		2dFGRS		6dFGS		2QZ/6QZ		NED	SIMBAD	Selected Value		RM (rad m ⁻²)
	z	Class	z	Class	z	Class ^a	z	Class	z	z	Source	z	
(1)	(2)	(3)	(4)	(5)	(6)	(7)	(8)	(9)	(10)	(11)	(12)	(13)	(14)
J000010+305559	1.801	1.8	NED	1.801	-37.9 ± 11.0
J000030-112119	0.10285	A(iv)	6dFGS	0.10285	+6.4 ± 12.4
J000132+145609	0.39878	B	0.39892	...	SDSS	0.39878	-34.9 ± 3.8
J000153-302508	1.30252	B	1.30252	...	6dFGS	1.30252	-0.1 ± 6.2
J000154+020453	0.402	...	NED	0.402	-14.9 ± 10.5
J000255-265451	0.0667	B	0.06666	B	0.06659	0.0665	6dFGS	0.06666	+0.8 ± 7.2
J000322-172711	1.465	...	NED	1.465	-33.2 ± 2.4
J000325-272631	0.2501	B	2dFGRS	0.2501	+1.9 ± 12.3
J000327-154706	0.508	0.508	NED	0.508	-2.8 ± 4.0
J000342-115149	1.30999	B	1.30999	...	6dFGS	1.30999	-3.8 ± 13.3

Note. — Table 3 is published in its entirety in the electronic edition of *The Astrophysical Journal Supplement Series*. The first 10 rows are shown here for guidance regarding its form and content.

^a The high proportion of 6dFGS and B class detections compared to the catalog as a whole is due to the low RAs of this sample (cf. Figure 1.)

Table 4

The contents of our RM-redshift catalog, compiled from four optical surveys and two databases, broken down by association class.

Class	SDSS	2dFGRS	6dFGS	2QZ/6QZ	NED	SIMBAD	All	Selected	Selected, $ b \geq 20^\circ$
A.....	1135	15	23	27	1200	1162	1160
A(i).....	528	6	11	16	561	539	538
A(ii).....	12	0	0	1	13	12	12
A(iii).....	225	3	5	3	236	231	231
A(iv).....	83	2	2	2	89	86	86
A(v).....	220	4	3	5	232	225	224
A(vi).....	17	0	2	0	19	19	19
A(vii).....	50	0	0	0	50	50	50
B.....	77	43	236	35	391	375	345
C.....	174	9	19	3	205	195	193
D.....	3186	...	3186	2023	1742
E.....	1907	1907	248	210
Total.....	1386	67	278	65	3186	1907	6889	4003	3650
Selected.....	1380	44	264	44	2023	248	4003	N/A	N/A
Selected, $ b \geq 20^\circ$	1376	44	234	44	1742	210	3650	N/A	N/A

Note. — The row labelled ‘Total’ gives the total number of associations made between Taylor et al. (2009) sources and the optical survey or database in question, while the rows labelled ‘Selected’ indicate the number of cases where this survey or database is the source of the ‘selected redshift’ (see §3.3) — for example, there are many cases for which the same Taylor et al. (2009) source has a redshift in both SDSS and NED, in which case the SDSS redshift is selected over the NED one. The column labelled ‘All’ lists the total number of times a given association class is assigned to a match between a Taylor et al. (2009) source and an optical counterpart, while the columns labelled ‘Selected’ indicate the number of selected redshifts in each association class — for example, most SIMBAD matches (class E) also have another match in class A, B or C from an optical survey.

Table 5

Selected Columns from Our RRM-Redshift Catalog of Polarized Radio Sources with Optical Counterparts

NVSS ID	ℓ	b	NVSS RM	Stokes I Flux	Frac Pol	Source	Class	Object	Redshift	GRM	RRM
(1)	($^\circ$)	($^\circ$)	(rad m^{-2})	(mJy)	(%)	(7)	(8)	Type	(10)	(rad m^{-2})	(rad m^{-2})
	(2)	(3)	(4)	(5)	(6)			(9)		(11)	(12)
J000010+305559	110.15	-30.66	-37.9 ± 11.0	88.2 ± 2.7	6.5 ± 0.3	NED	D	Quasar	1.801 ± 0.007	-74.2 ± 7.5	$+36.3 \pm 13.3$
J000030-112119	83.29	-70.20	$+6.4 \pm 12.4$	80.9 ± 2.9	6.8 ± 0.4	6dFGS	A(iv)	...	$0.10285 \pm \dots$	$+1.9 \pm 4.1$	$+4.5 \pm 13.1$
J000132+145609	105.37	-46.23	-34.9 ± 3.8	314.6 ± 11.1	5.5 ± 0.1	SDSS	B	Quasar	$0.39878 \pm \dots$	-28.9 ± 5.2	-6.0 ± 6.4
J000153-302508	13.14	-78.66	-0.1 ± 6.2	173.8 ± 5.2	6.4 ± 0.2	6dFGS	B	...	$1.30252 \pm \dots$	$+15.4 \pm 4.1$	-15.5 ± 7.4
J000154+020453	98.76	-58.45	-14.9 ± 10.5	300.7 ± 9.7	3.3 ± 0.2	NED	D	Galaxy	$0.402 \pm \dots$	-8.3 ± 5.4	-6.6 ± 11.8
J000255-265451	31.30	-79.20	$+0.8 \pm 7.2$	94.4 ± 3.2	12.8 ± 0.4	6dFGS	B	...	$0.06666 \pm \dots$	$+4.9 \pm 3.9$	-4.1 ± 8.2
J000322-172711	71.53	-75.28	-33.2 ± 2.4	2414.8 ± 72.4	1.5 ± 0.0	NED	D	Quasar	1.465 ± 0.003	$+1.9 \pm 4.6$	-35.1 ± 5.2
J000325-272631	28.49	-79.33	$+1.9 \pm 12.3$	144.0 ± 5.1	5.2 ± 0.3	2dFGRS	B	...	$0.2501 \pm \dots$	$+5.9 \pm 4.1$	-4.0 ± 13.0
J000327-154706	76.02	-74.10	-2.8 ± 4.0	527.3 ± 15.8	3.2 ± 0.1	NED	D	Galaxy	$0.508 \pm \dots$	-5.4 ± 3.4	$+2.6 \pm 5.3$
J000342-115149	84.35	-71.07	-3.8 ± 13.3	351.7 ± 12.2	1.6 ± 0.1	6dFGS	B	...	1.30999 ± 0.0068	-2.4 ± 3.3	-1.4 ± 13.7

Note. — Table 5 is published in its entirety in the electronic edition of *The Astrophysical Journal Supplement Series*. The first 10 rows are shown here for guidance regarding its form and content.

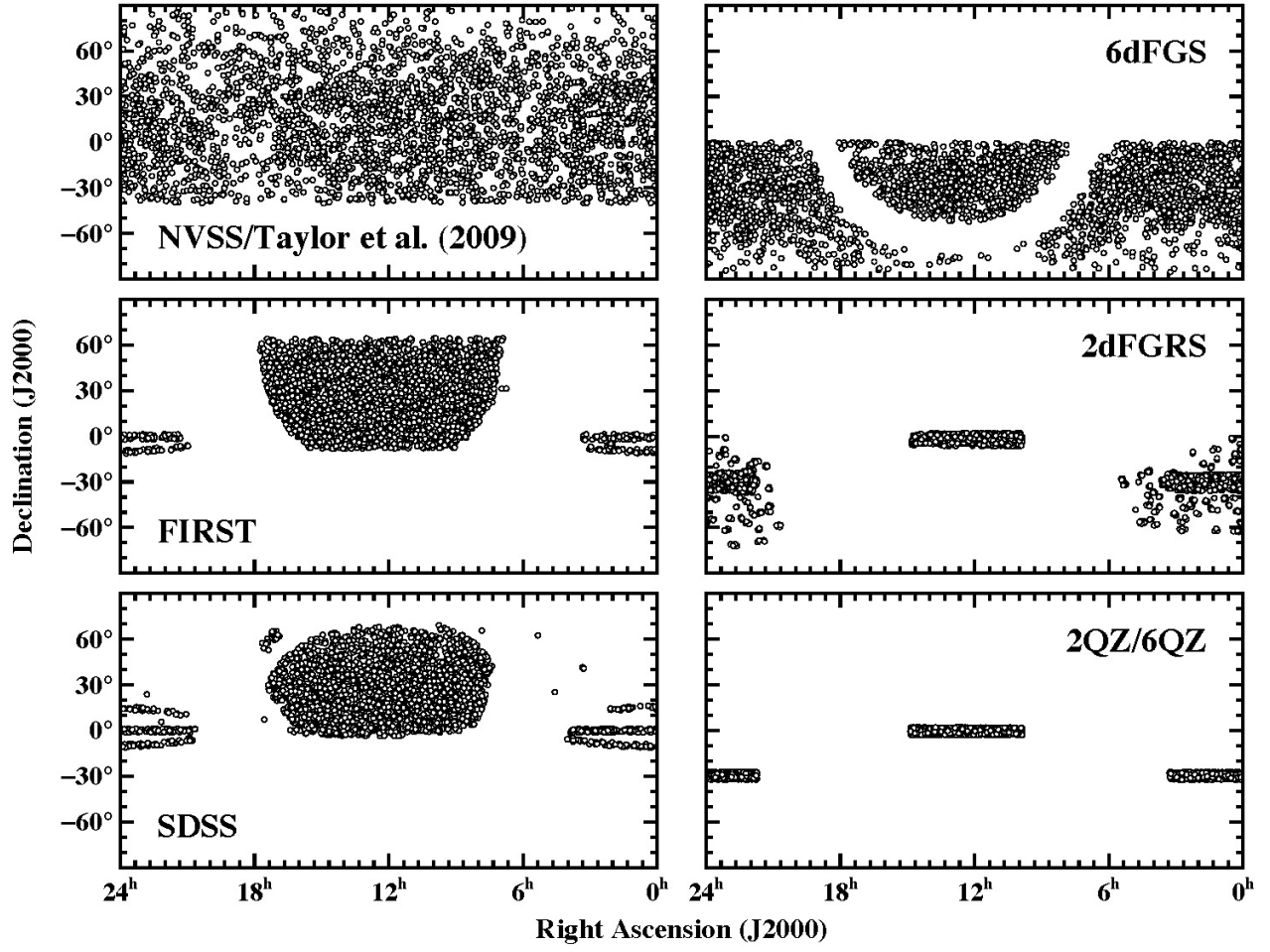


Figure 1. The sky coverage for each of the surveys used in the creation of our RM vs. redshift catalog, shown using sparse sampling.

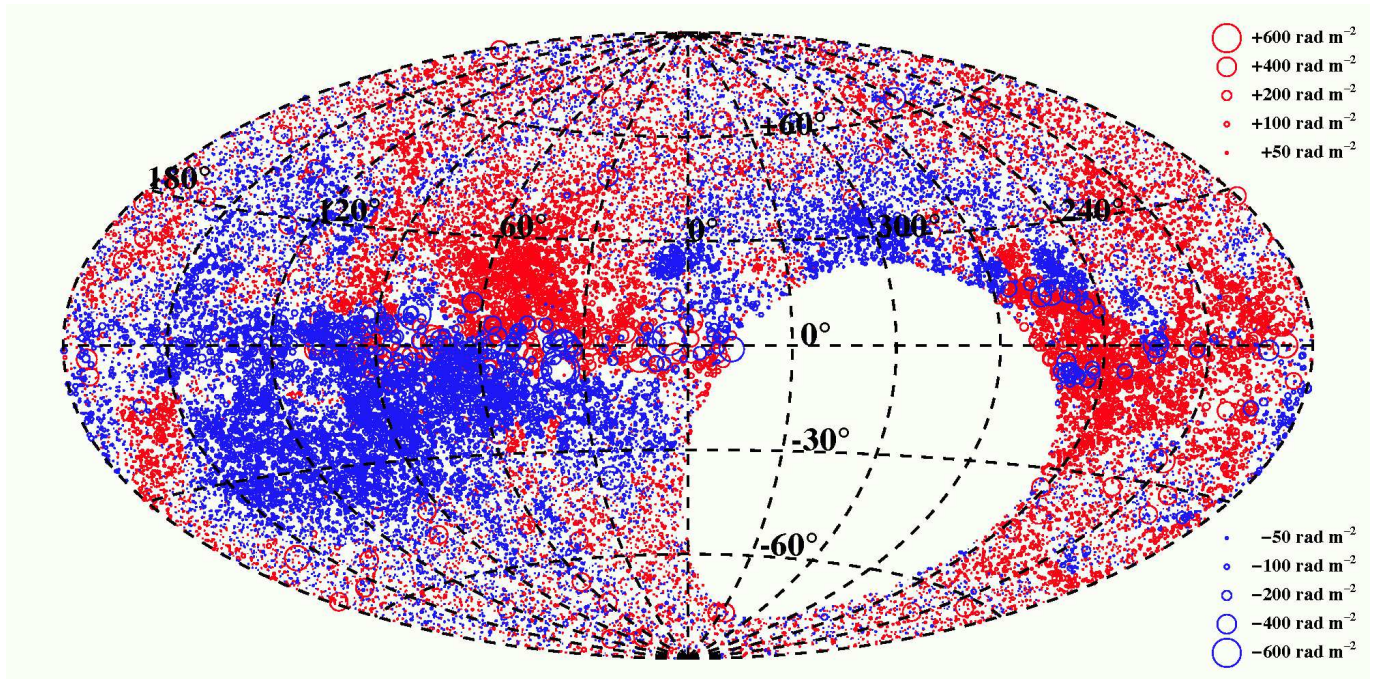


Figure 2. RMs of 37 543 extragalactic sources over the sky above a declination of -40° from the survey by Taylor et al. (2009). Red circles correspond to positive RMs while blue circles are negative. The size of the circle scales linearly with the magnitude of the RM. The sources are mapped onto a Galactic co-ordinate system.

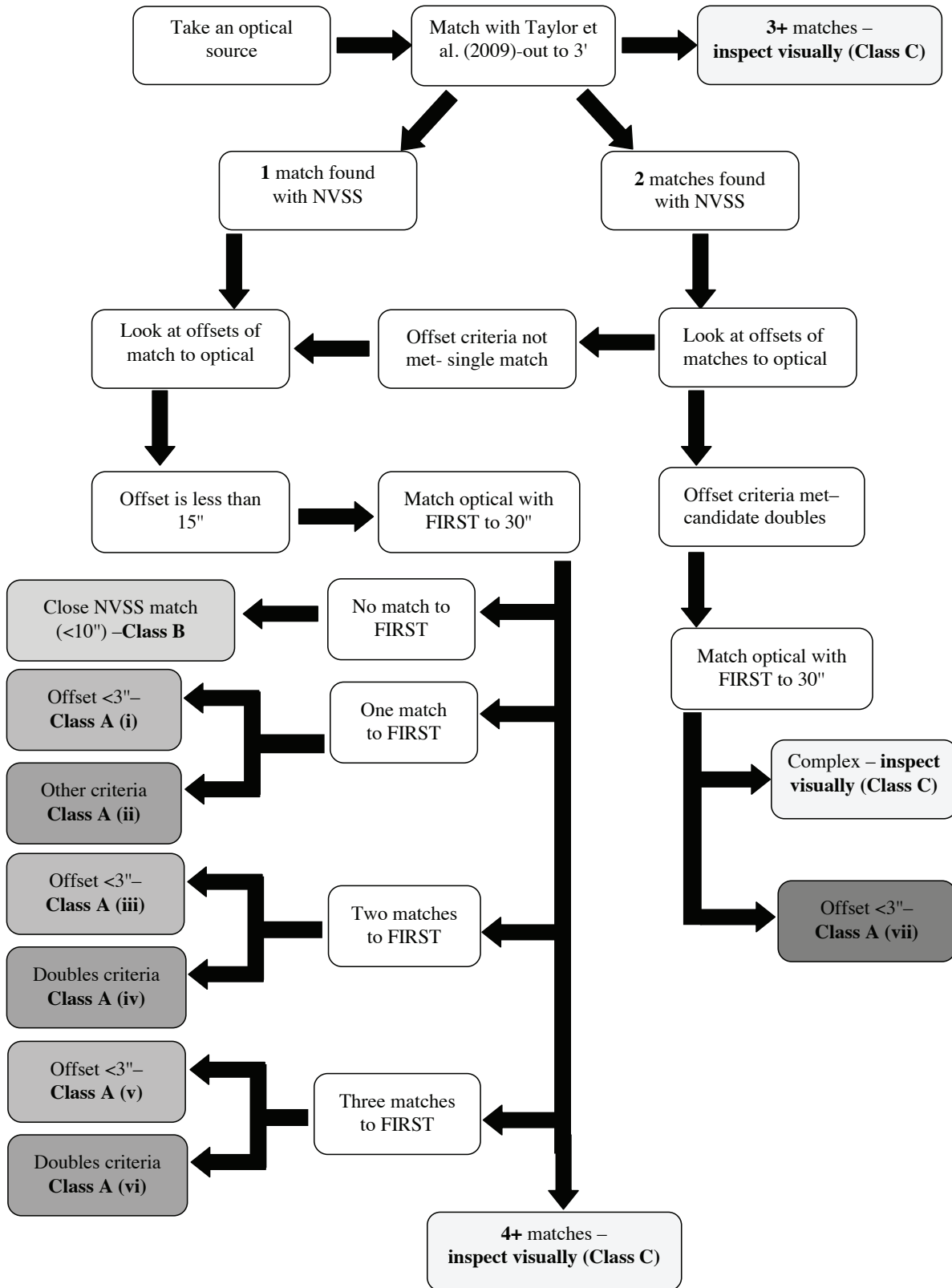


Figure 3. A simplified flowchart representation of the algorithm implemented in this paper to make associations between optical and radio sources in various surveys. Final association classes are shown shaded, with the same shading used for classes with similar admission criteria.

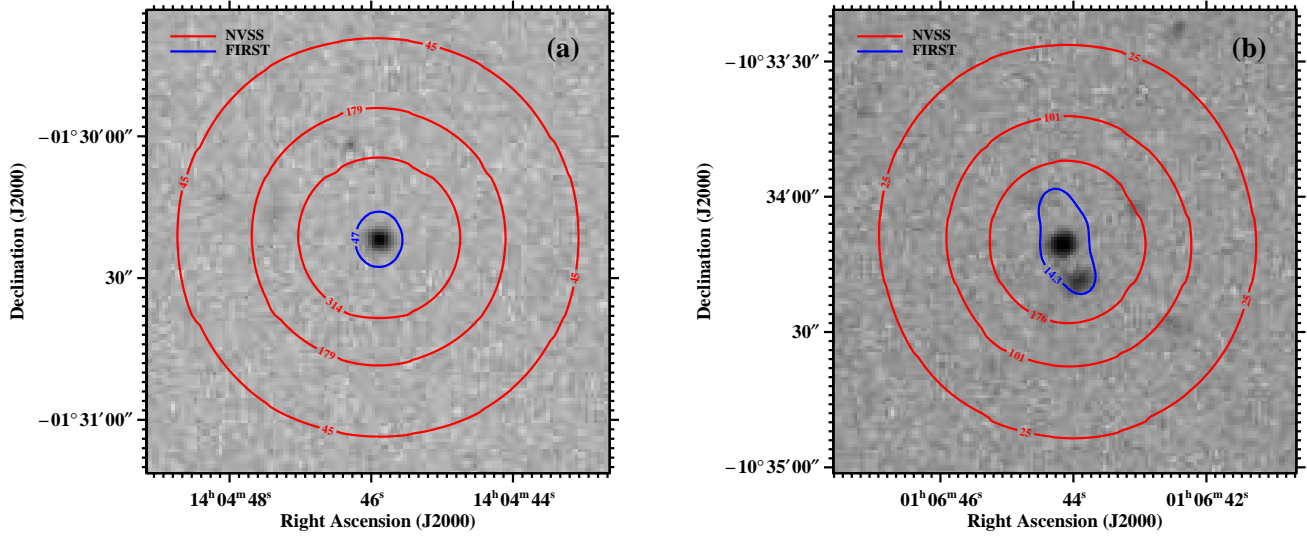


Figure 4. Examples of class A(i) associations (close core match with FIRST data) made with our algorithm. Optical data are shown in gray-scale with NVSS radio contours overlaid in red and FIRST radio contours overlaid in blue. (a) NVSS J140445-013021: class A(i) association for both SDSS and 2QZ/6QZ. (b) NVSS J010644-103409: class A(i) association for both SDSS and 6dFGS. All contour levels are measured in mJy beam^{-1} . In this and subsequent related Figures, optical data are taken from SDSS where available, and otherwise from SuperCOSMOS.

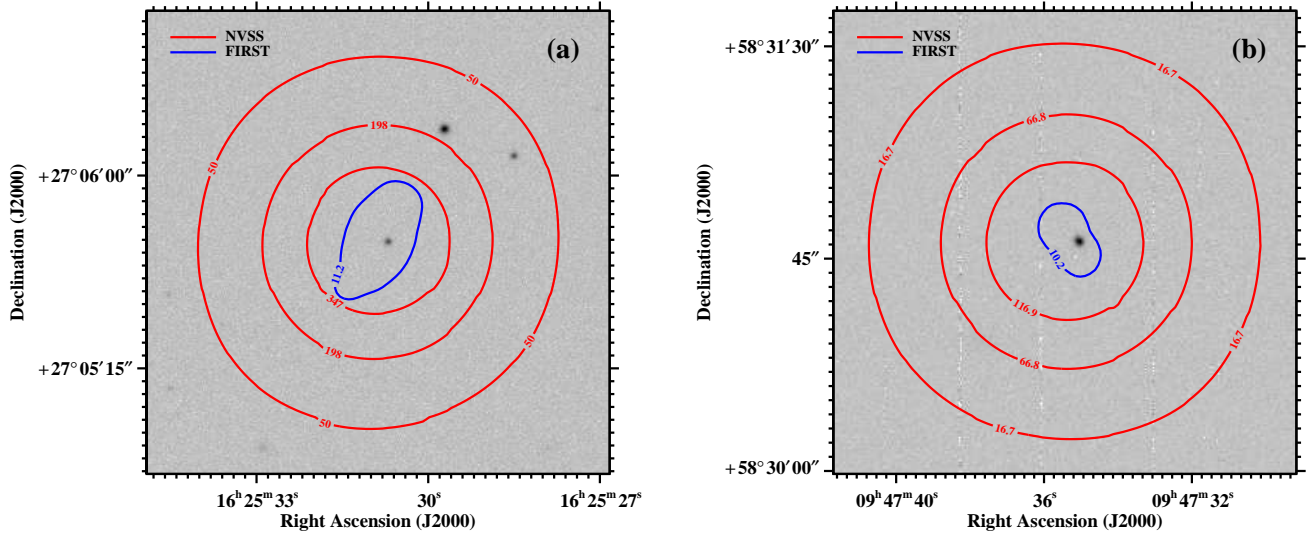


Figure 5. As for Figure 4, but showing examples of class A(ii) associations (core match with FIRST data). (a) NVSS J162530+270544: class A(ii) association with the SDSS. (b) NVSS J094735+583048: class A(ii) association with the SDSS.

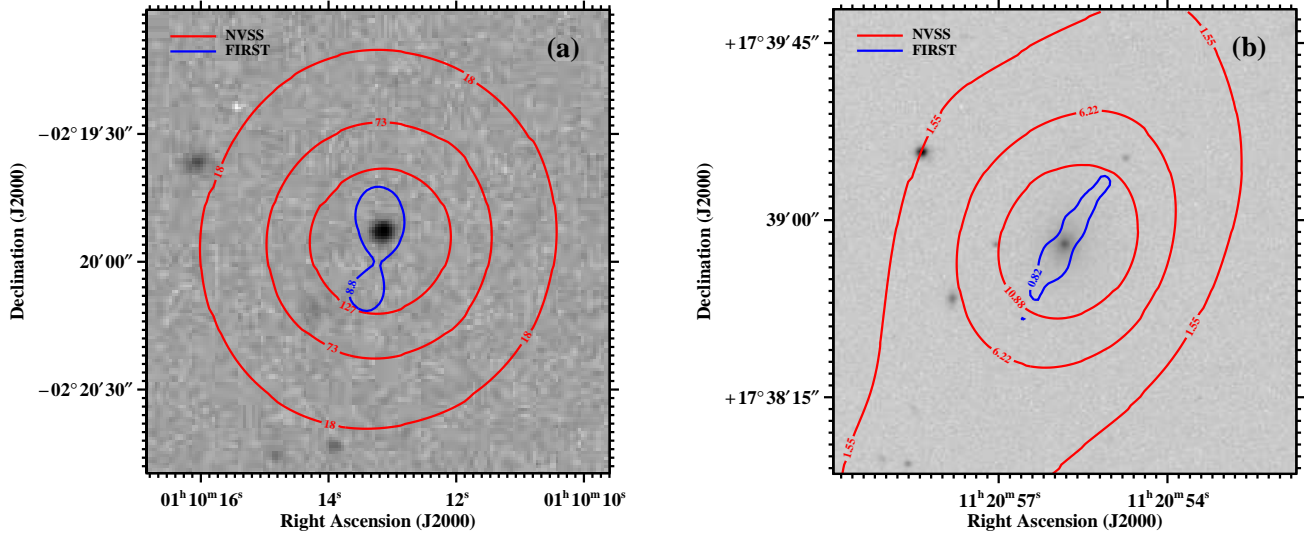


Figure 6. As for Figure 4, but showing examples of class A(iii) associations (single NVSS source, closely matched double source seen with FIRST). (a) NVSS J011013-021954: class A(iii) association with the 6dFGS. (b) NVSS J112055+173854: class A(iii) association with the SDSS.

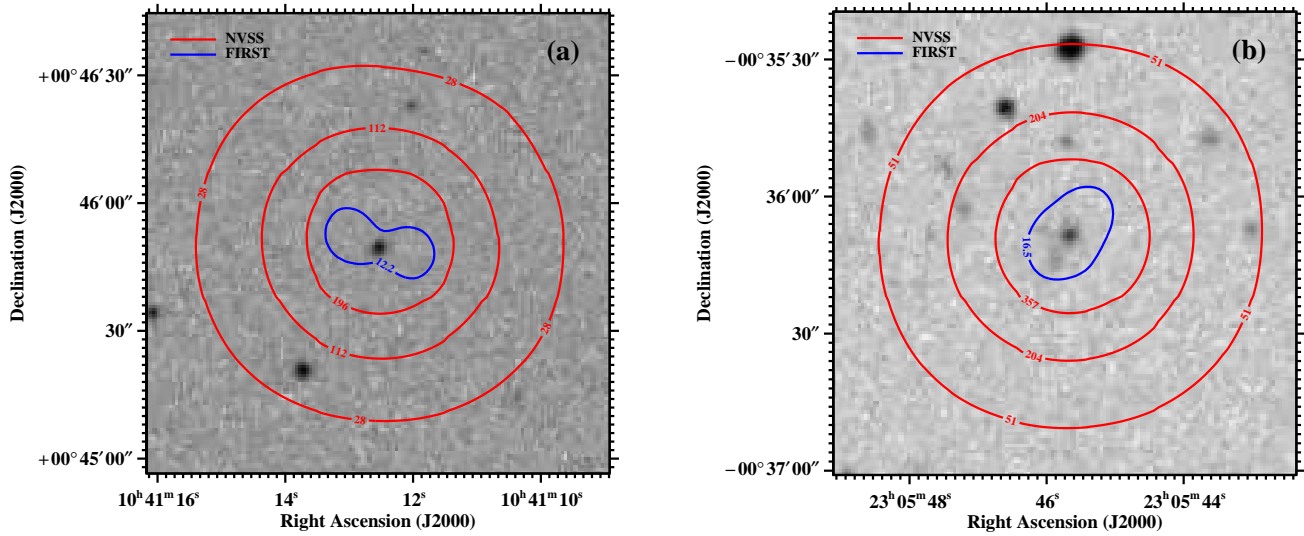


Figure 7. As for Figure 4, but showing examples of class A(iv) associations (single NVSS source, double source seen with FIRST). (a) NVSS J104112+004550: class A(iv) association with the 2QZ/6QZ. (b) NVSS J230545-003608: class A(iv) association with the SDSS and 2dFGRS.

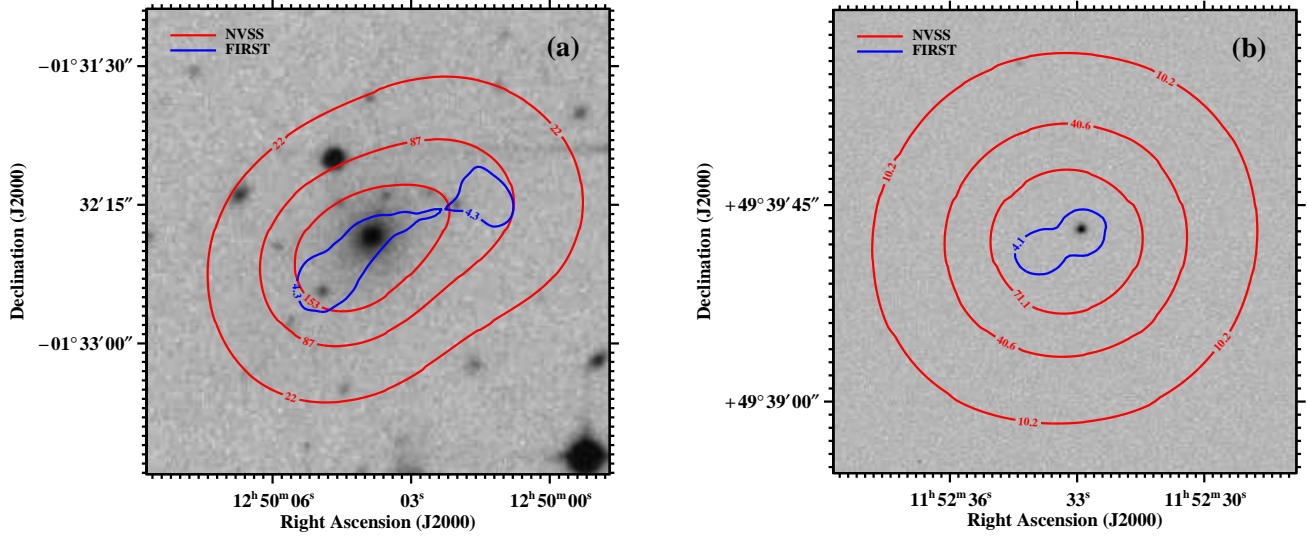


Figure 8. As for Figure 4, but showing examples of class A(v) associations (single NVSS source, closely matched triple source seen with FIRST). (a) NVSS J125003-013226 : class A(v) association with the 2dFGRS. (b) NVSS J115233+493937: class A(v) association with the SDSS.

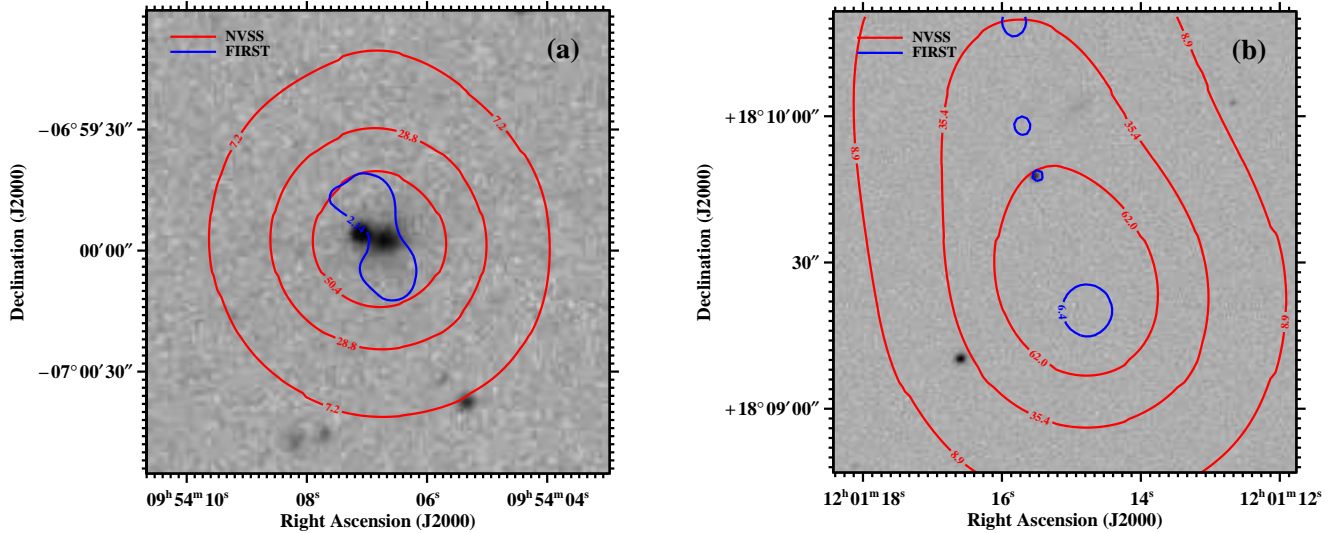


Figure 9. As for Figure 4, but showing examples of class A(vi) associations (single NVSS source, triple source seen with FIRST). (a) NVSS J095406-065957: class A(vi) association with the 6dFGS. (b) NVSS J120115+180934: class A(vi) association with the SDSS; here, the faint optical source lies within the second FIRST component from the bottom.

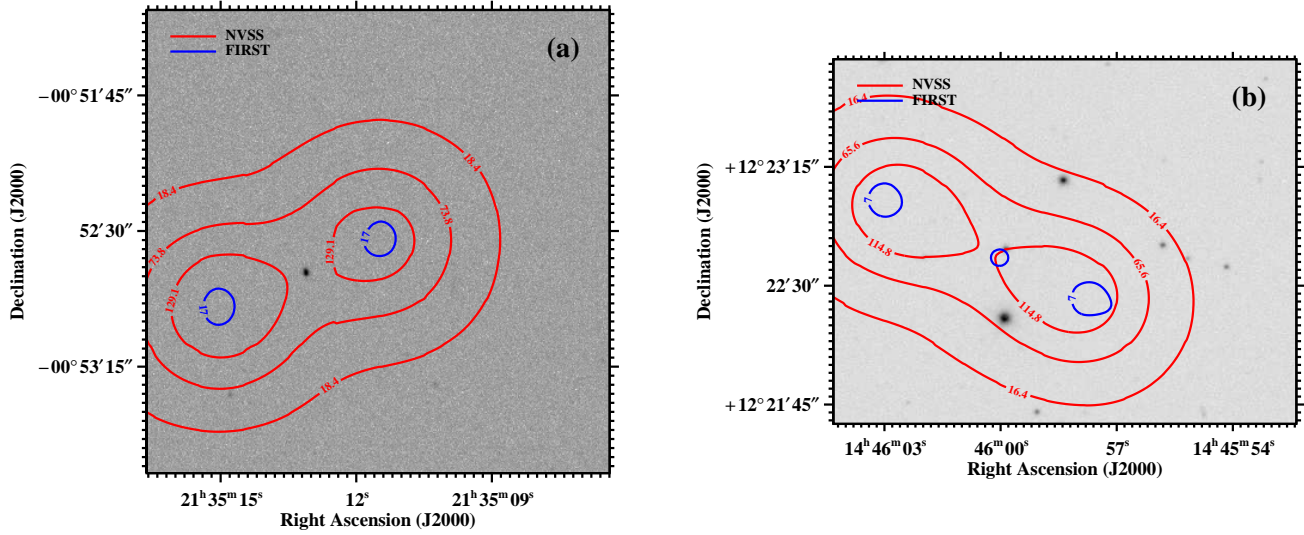


Figure 10. As for Figure 4, but showing examples of class A(vii) associations (double-lobed radio source in NVSS, also detected in FIRST). (a) NVSS J213515–005255 and NVSS J213511–005233: class A(vii) association with the SDSS; the optical source lies in the middle of the FIRST contours. (b) NVSS J144558+122228 and NVSS J144602+122258: class A(vii) association with the SDSS.

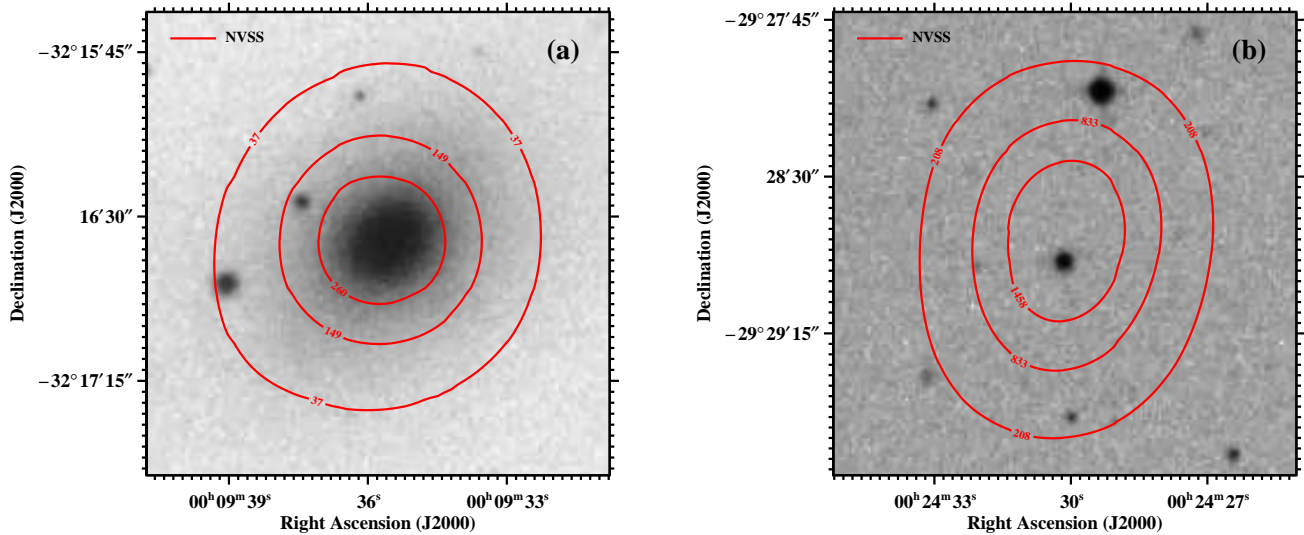


Figure 11. As for Figure 4, but showing examples of class B associations (core match with NVSS but either no FIRST detection or no FIRST observations). (a) NVSS J000935–321636: class B association for both 6dFGS and 2dFGRS. (b) NVSS J002430–292848: class B association with the 2QZ/6QZ; in this case, the optical source is slightly offset from the radio center.

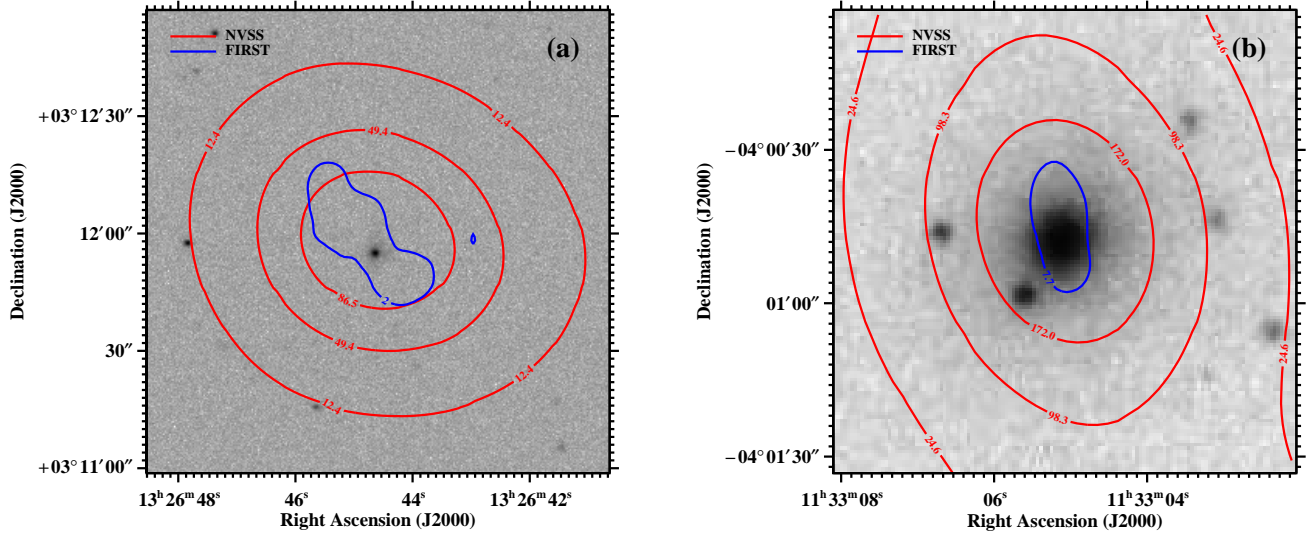


Figure 12. As for Figure 4, but showing examples of class C associations (complex sources requiring manual visual inspection). (a) NVSS J132644+031158: class C association with the SDSS; here the complexity is the presence of four FIRST components. (b) NVSS J113305-040047: class C association with the 6dFGS; the complexity here is the extremely extended nature of the NVSS source, which FIRST does not detect.

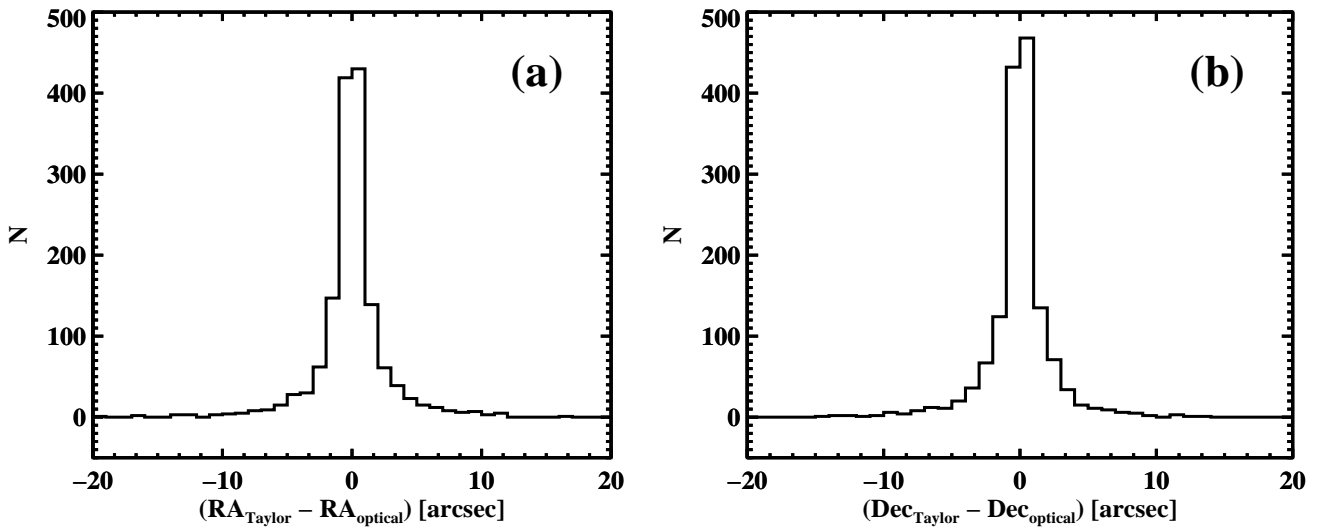


Figure 13. Histograms showing the distribution of radio and optical positional offsets in our RM-redshift catalog in (a) Right Ascension and (b) Declination. The catalog includes a small number of associations with offsets outside the range shown (these sources, like all those beyond an offset of $\approx 7''$, have a double-lobed or complex radio morphology, leading to large separations between radio and optical source positions).

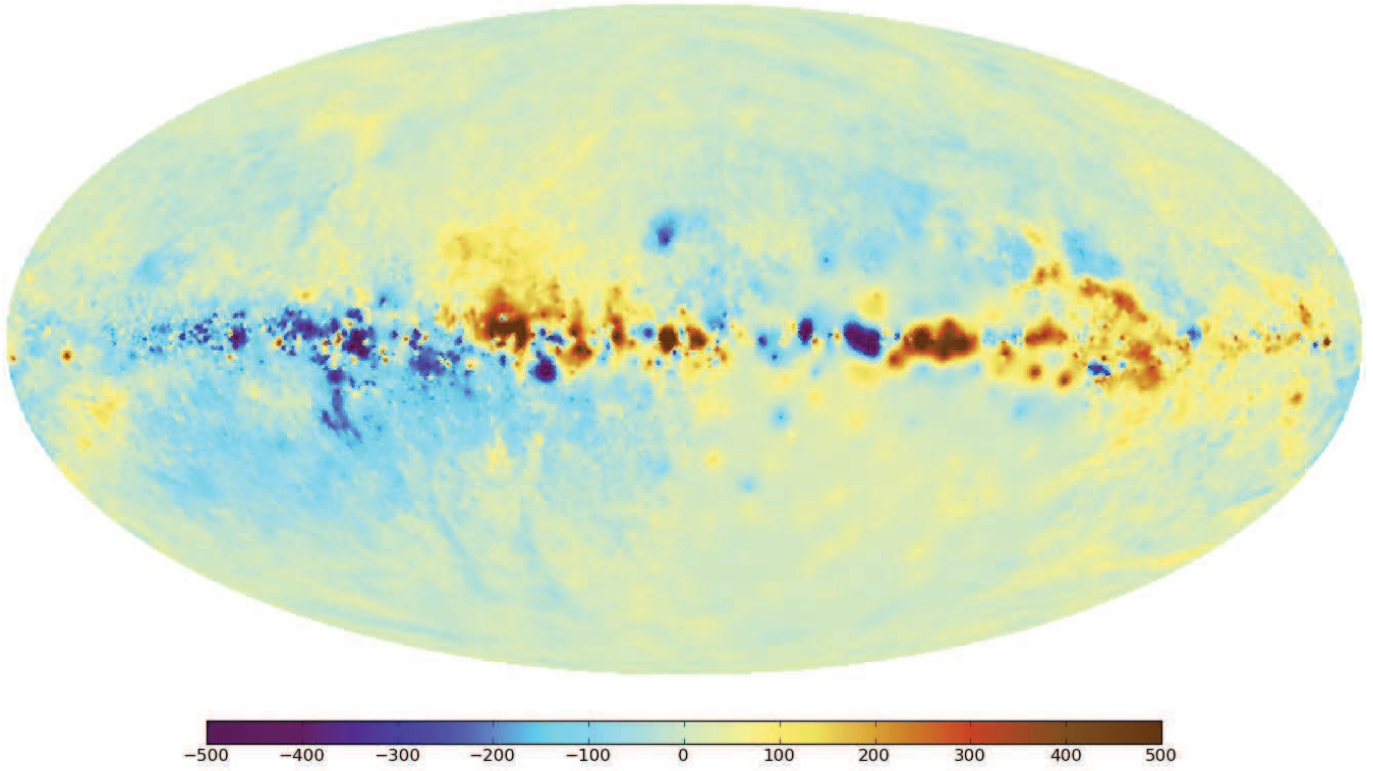


Figure 14. Map of the foreground Faraday sky in rad m^{-2} by Oppermann et al. (2012).

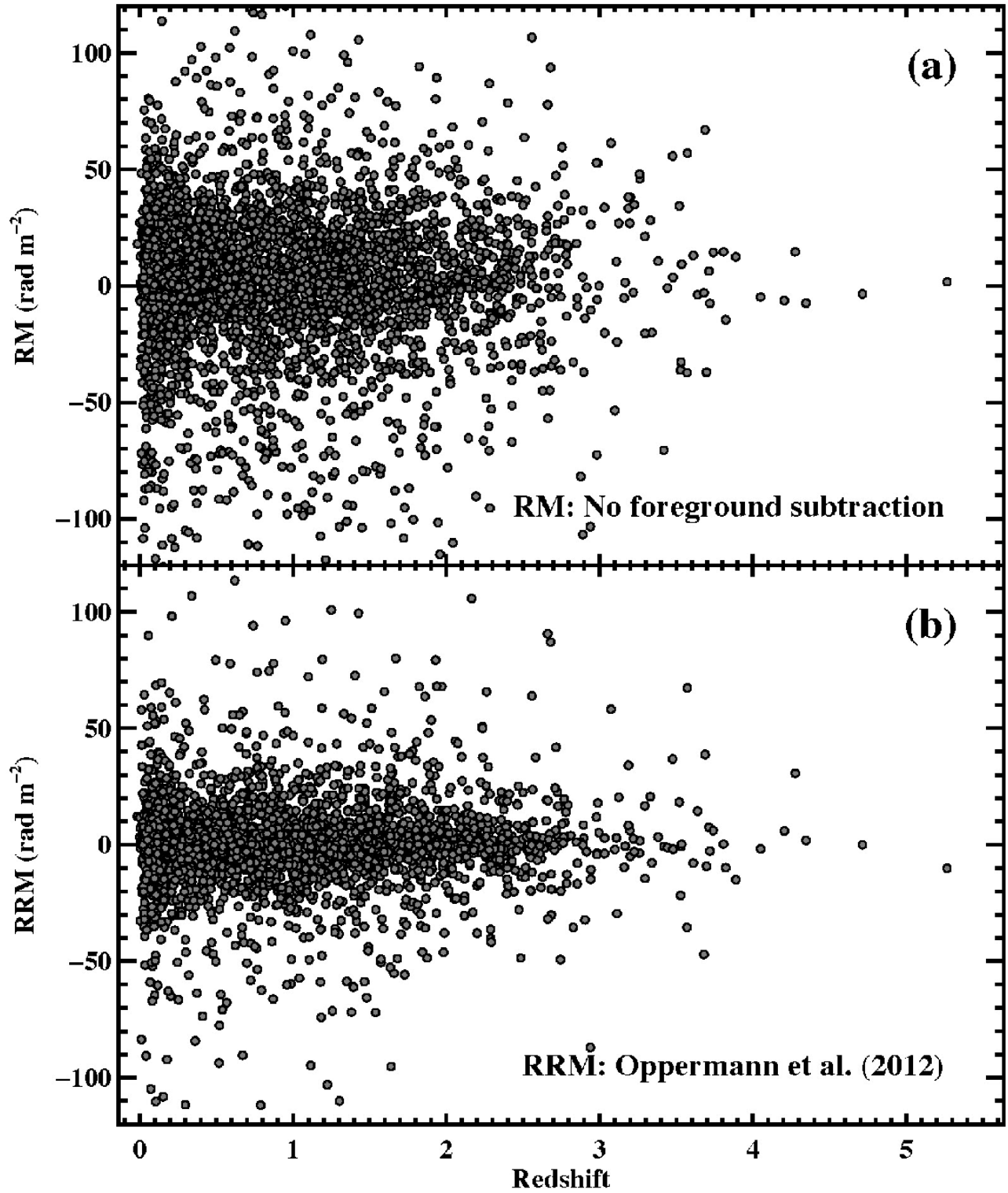


Figure 15. Comparison of (a) RM vs. z and (b) RRM vs. z , showing the impact of the GRM subtraction.

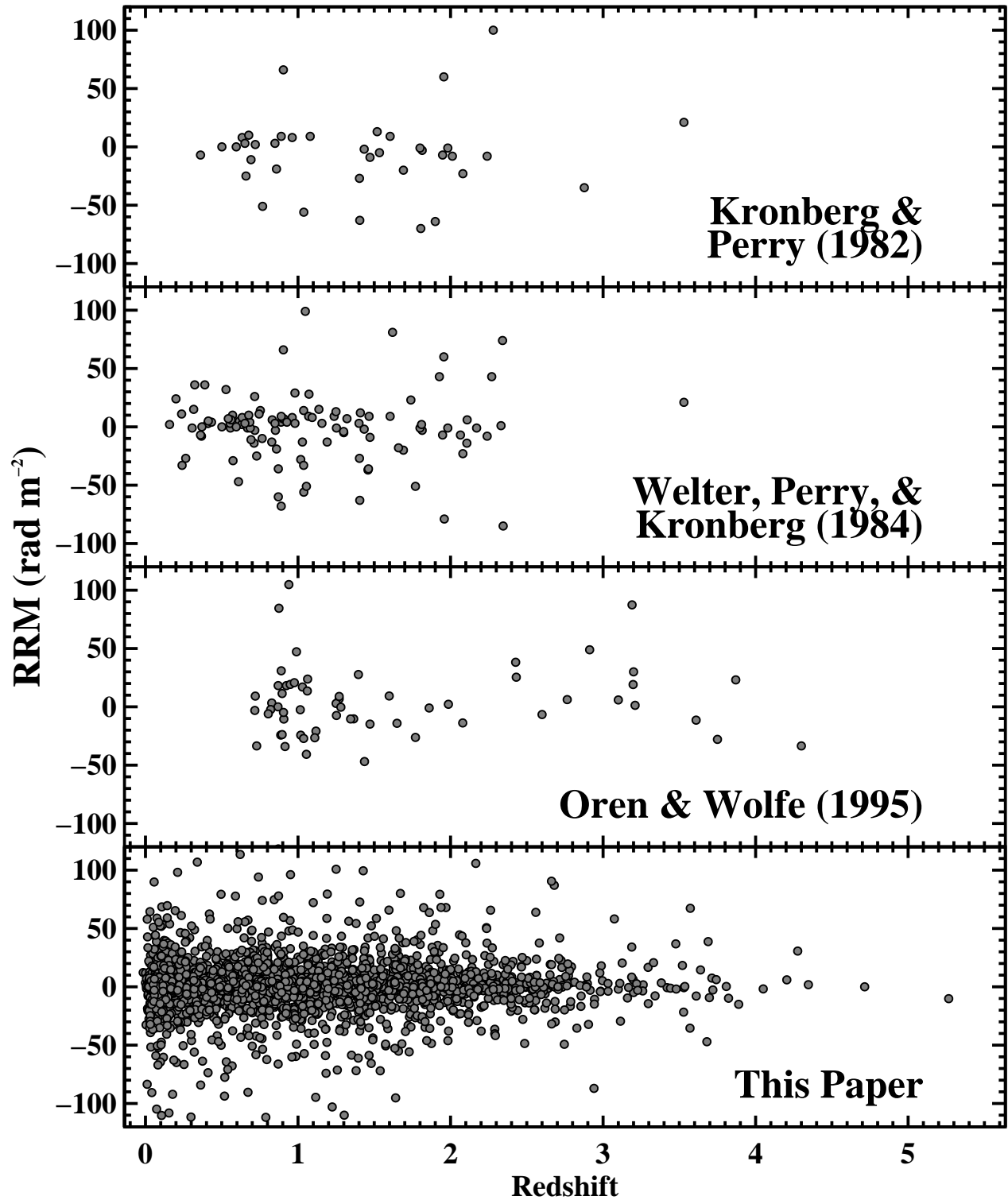


Figure 16. A comparison of our RRM-redshift catalog (bottom panel) with previously published data sets. A catalog of 268 objects discussed by Kronberg et al. (2008) has not yet been made available.

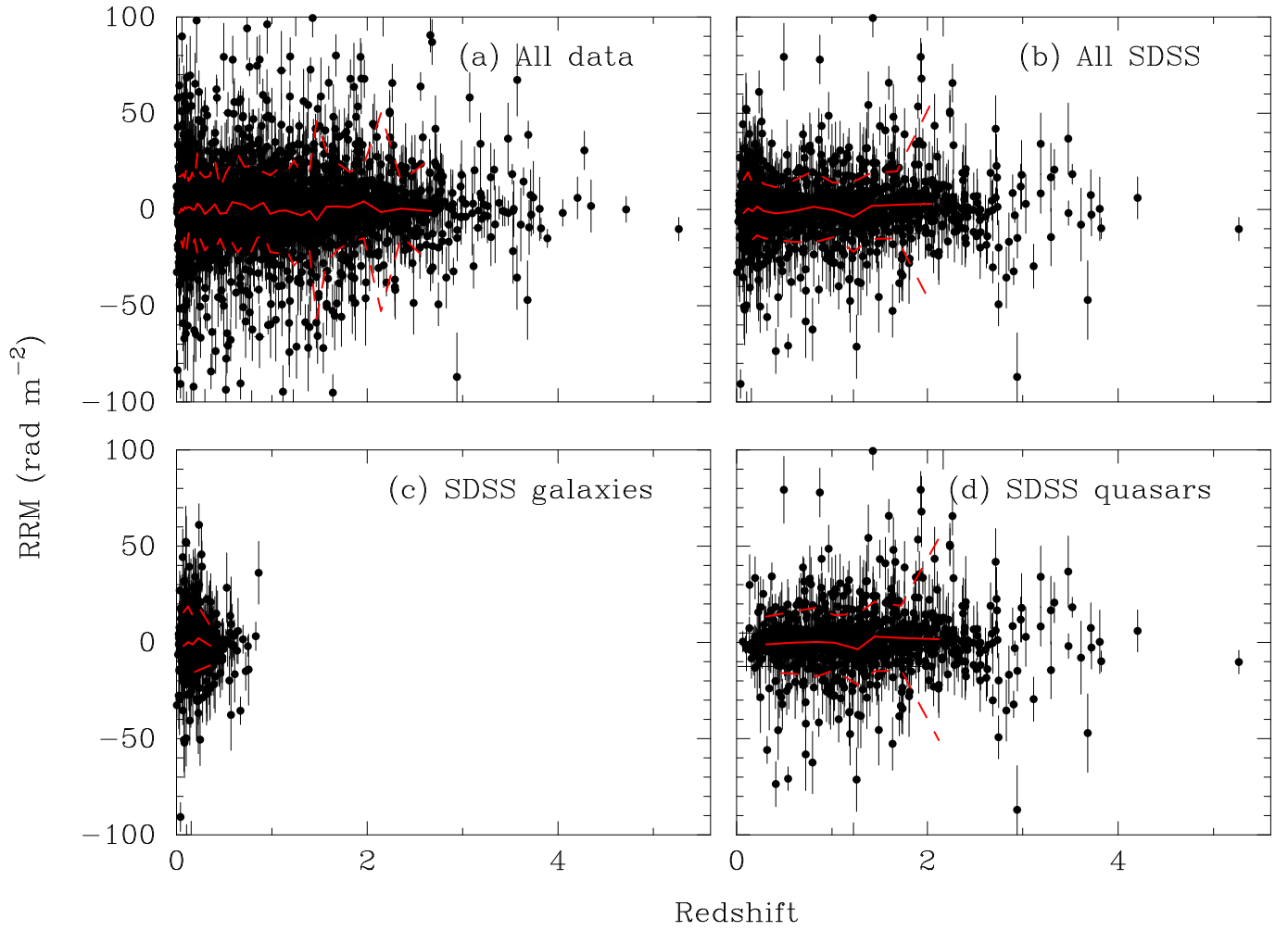


Figure 17. RRM vs. redshift for (a) the whole RRM-redshift catalog of 3650 sources, (b) the subset of 1376 sources with selected redshifts from the SDSS, (c) the 516 galaxies with selected redshifts from the SDSS, and (d) the 860 quasars with selected redshifts from the SDSS. In each panel, individual data points are shown in black, while the mean RRM and $\pm 1\sigma$ values of RRM on either side of this mean in independent adjacent bins of 50 points are shown by the solid red line and the dashed red lines, respectively. Note that there are 15 sources with $\text{RRM} < -100 \text{ rad m}^{-2}$ and 10 sources with $\text{RRM} > +100 \text{ rad m}^{-2}$ that are outside the range plotted.

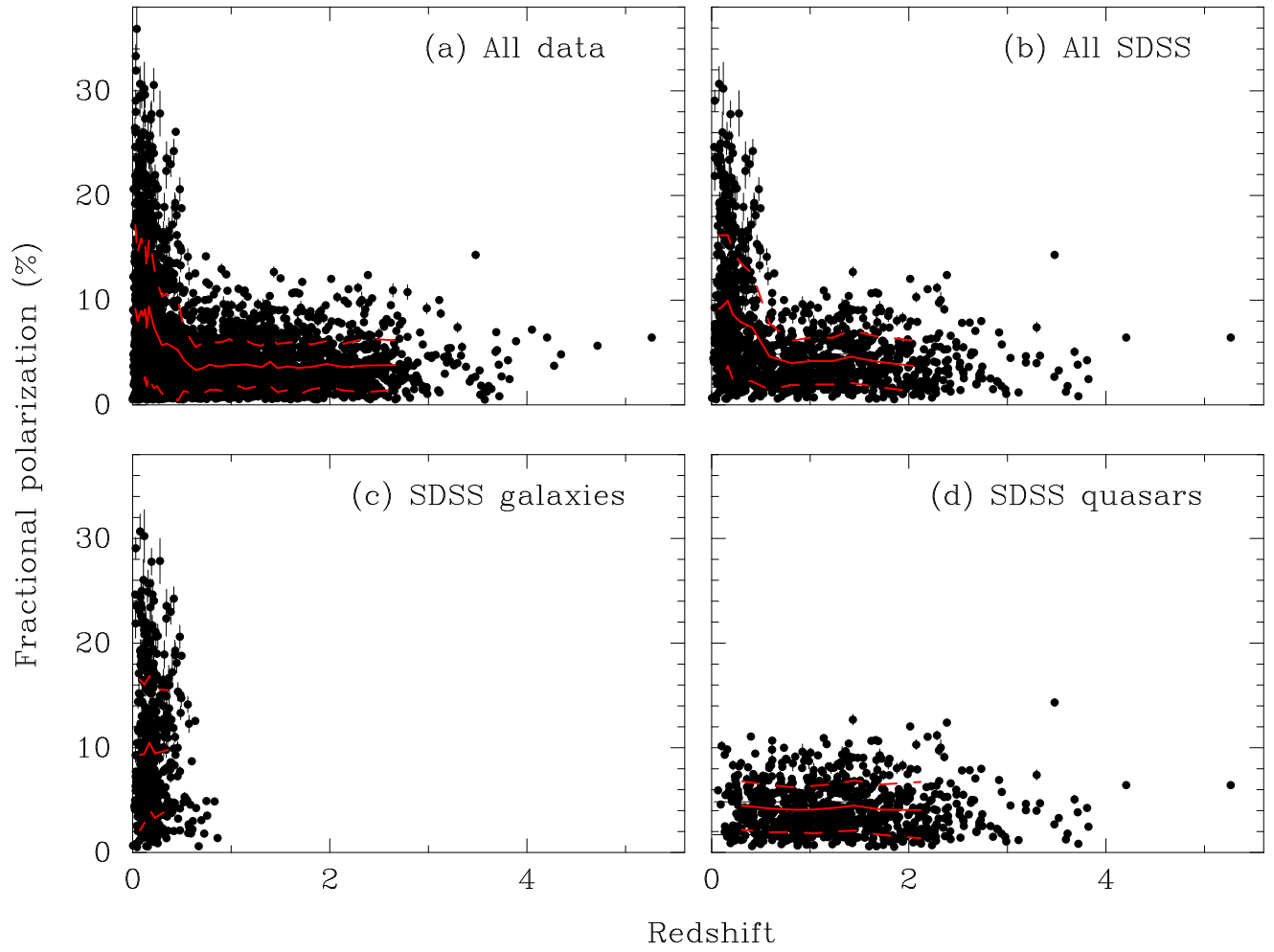


Figure 18. As for Figure 17, but showing fractional polarization vs. redshift.

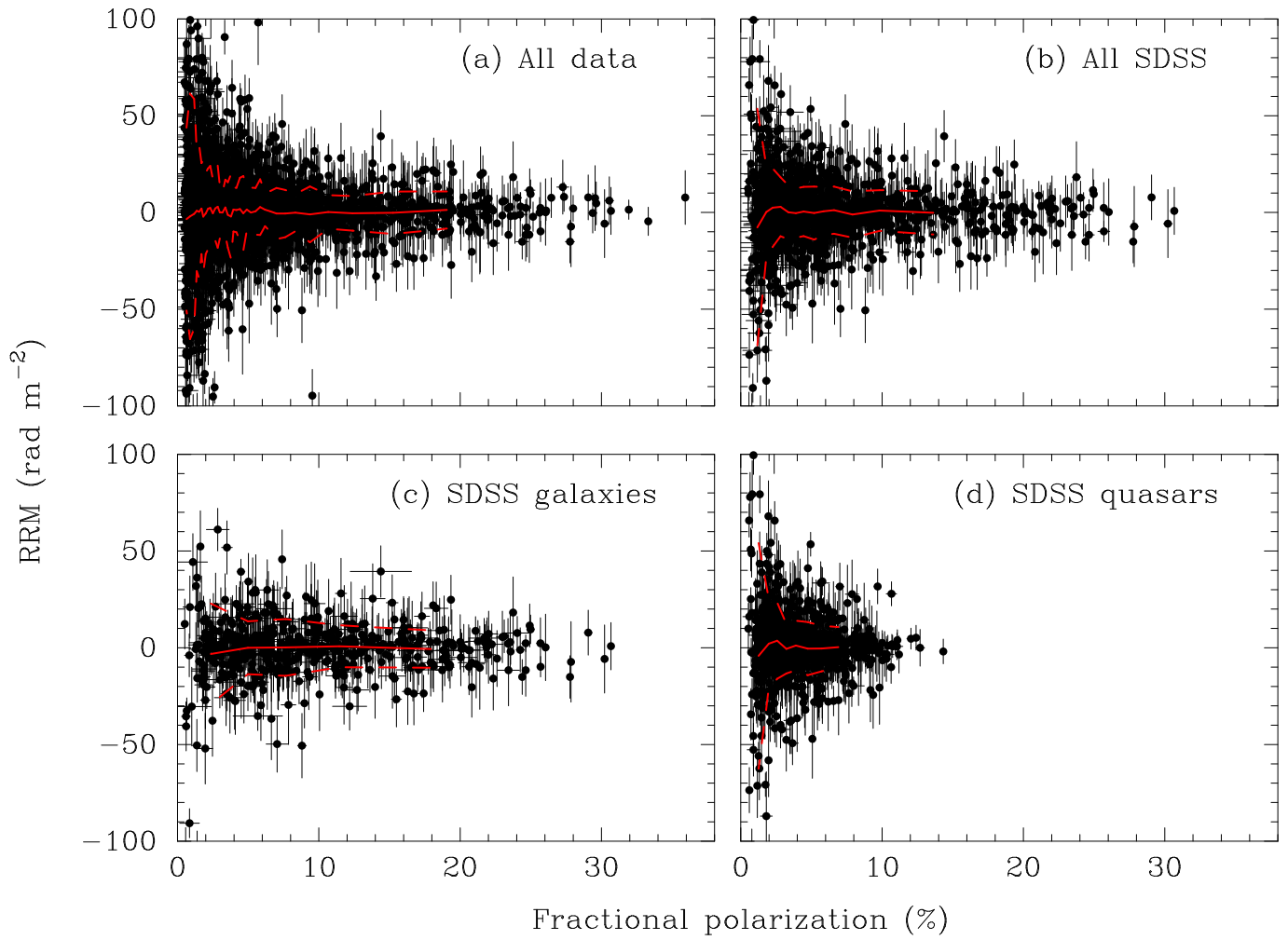


Figure 19. As for Figure 17, but showing RRM vs. fractional polarization. There are 15 sources with $\text{RRM} < -100 \text{ rad m}^{-2}$ and 10 sources with $\text{RRM} > +100 \text{ rad m}^{-2}$ that are outside the range plotted.